

# A WISE Census of Young Stellar Objects in Perseus OB2 Association

Mohaddesseh Azimlu<sup>1</sup>; J. Rafael Martinez-Galarza<sup>1</sup>; August A., Muench<sup>1</sup>

## ABSTRACT

We have performed a *WISE* (Wide-Field Infrared Survey Explorer) based study to identify and characterize young stellar objects (YSOs) in  $12^\circ \times 12^\circ$  Perseus OB 2 association. Spectral energy distribution (SED) slope in range of  $3.4 - 12\mu\text{m}$  and a  $5\sigma$  selection criteria were used to select our initial sample. Further manual inspection reduced our final catalog to 156 known and 119 YSO candidate. The spatial distribution of newly found YSOs all over the field shows an older generation of star formation which most of its massive members have evolved into main sequence stars. In contrast, the majority of younger members lie within the Perseus molecular cloud and currently active star forming clusters such as NGC 1333 and IC 348. We also identified additional 66 point sources which passed YSO selection criteria but are likely AGB stars. However their spatial distribution suggests that they may contain a fraction of the YSOs. Comparing our results with the commonly used color-color selections, we found that while color selection method fails in picking up bright but evolved weak disks, our SED fitting method can identify such sources, including transitional disks. In addition we have less contamination with background sources such as galaxies, but in a price of loosing fainter ( $J_{mag} > 12$ ) YSOs. Finally we employed a Bayesian Monte Carlo SED fitting method to determine the characteristics of each YSO candidate. Distribution of SED slopes and model driven age and mass confirms separated YSO populations with suggested three age groups of younger than 1 Myr old, 1 – 5 Myr old, and older than 5 Myrs which agrees with the age of Per OB 2 association and currently star forming sites within the cloud.

## 1. INTRODUCTION

Perseus is one of the most interesting and well studied star forming complexes, containing massive stars (Per OB2 association), young stellar clusters (e.g. IC348 and NGC1333) and several dense star forming cores within Perseus molecular cloud (e.g. Kirk et al. (2006); Ridge et al. (2006); Rosolowsky et al. (2008)). Perseus OB2 is the second closest OB association to the Sun (after Scorpius-Centaurus association) at a distance of  $\sim 300$  pc. de Zeeuw et al. (1999) estimated that Per OB2 is approximately 6 Myr old while other studies also suggest different generation of star formation with an age less than 15 Myr (e.g. Bally et al. (2008) and references therein).

Per OB2 contains both massive and intermediate mass stars while low mass to intermediate mass stars are currently forming within the Perseus molecular cloud (e.g. Enoch et al. (2009); Arce et al. (2010); Sadavoy et al. (2014)). Therefore identifying the members of the association and determining

---

<sup>1</sup>Harvard-Smithsonian Center for Astrophysics, Cambridge, MA 02138

their characteristics such as their age and mass will provide critical information on the process of different generations of star formation in this region.

We constructed a panchromatic census of young stellar objects (YSOs) in Per OB2 using Wide-field Infrared Survey Explorer (*WISE*) point source catalogue. We also employed all available optical and infrared all sky surveys including *Spitzer*, 2MASS and SDSS to construct spectral energy distribution (SED) of each source in order to determine its physical parameters. We have performed a *WISE* based survey to identify young stellar objects throughout a  $12^\circ \times 12^\circ$  area covering the Per OB2 association.

The Perseus molecular cloud covers a  $2^\circ \times 6^\circ$  ( $\sim 10 \times 30$  pc) area and was observed with the *Spitzer* space observatory in both IRAC ( $3.6 - 8.0 \mu\text{m}$ ) and MIPS ( $24 - 160 \mu\text{m}$ ) as part of “From Molecular Cores to Planet-Forming Disks” (c2d) Legacy Survey (Jørgensen et al. 2006; Rebull et al. 2007). We selected the c2d covered region as footprint, but did not limit our survey to the c2d area. c2d only covers very young star forming regions such as IC348 and NGC1333 clusters. To study the complete population of Perseus OB2 association we need to track all the members of the original ensemble, in particular the entire OB association which has blown up the initial molecular cloud and other young stellar objects, now spread into a larger area. Assuming an average speed of  $1 - 2 \text{ km s}^{-1}$  for stars, members can travel more than 20 pc in 10 Myrs in each direction which converts to an extended area of  $\sim 10^\circ$  from the cloud center at 250 – 300 pc distance.

To be complete, we selected a  $12^\circ \times 12^\circ$  region ( $50^\circ < \text{RA} < 64^\circ$  and  $26^\circ < \text{Dec} < 38^\circ$ ) around the Perseus c2d footprint which completely covers the Perseus OB2 association. This region slightly overlaps with Taurus star forming region in South-West and may contain older members of Pleiades in South as well. Figure 1 shows the c2d footprint, and the area selected around it in our survey. The Blue dots present *WISE* point sources. Unfortunately we do not have the spectral or dynamical data for each source, hence cannot confirm if each individual source in our final catalog is associated with the Per OB2 or the molecular cloud, but the luminosity and other parameters matches with the properties we expect for YSOs at the estimated distances. In addition, we are looking out of the Galactic plane and no other known background star forming region is along the line of sight. Foreground young stars, if any, would be much brighter than our criteria.

Section 2 explains the data collection and data reduction procedures. In section 4 we describe our YSO candidate selection method and compare the results with other YSO identification schemes. Section 4 contains the analysis of our sample of YSO candidates. In Section 5 we describe our SED fitting modeling and the results. We summarize this study in Section 6.

## 2. Archival Data and Data Reduction

To identify young stars we established a multi-wavelength database of point sources in Per OB2 star forming region, using all available large sky surveys. New YSO candidates then were selected through evidence for infrared excess in their spectral energy distributions (SED); specifically, we used power-law fits to the longer infrared wavelengths covered by the *WISE* all sky survey. In section 4 we detail the candidate selection procedure.

To summarize, *WISE* is an all sky survey in four infrared wavebands 3.4, 4.6, 12, and 22  $\mu\text{m}$  (hereafter W1, W2, W3 and W4) with an angular resolution of 6-6.5'' for W1 to W3 and 12.0'' for W4. The *WISE* depth is not homogenous, but achieved  $5\sigma$  point source sensitivities of 0.068, 0.098, 0.86 and 5.4 mJy (16.6, 15.6, 11.3, 8.0 Vega mag) in unconfused regions in the ecliptic plane for the four bands respectively. Our point source database was initially constructed using the *WISE* preliminary data release (Wright et al. 2010), but we upgraded to the final source release in March 2012. The  $12^\circ \times 12^\circ$  selected region in our census of Per OB2 includes more than 1.6 million *WISE* point sources (Figure 1).

After an initial inspection we realized that W4 sensitivity is very low for faint sources and in particular any W4 profile magnitude  $>8$  should be considered with caution. We therefore limited our search for infrared excess to the range of 3 – 12  $\mu\text{m}$ , and restricted our source list to have  $S/N > 7$  in the three corresponding W1, W2, and W3 bands. This criteria decreased the number of candidates to 65,662. We did not use the *WISE* catalog flags to further filter our candidate list because we found the flags to be unreliable; in particular many sources were not flagged as extended or questionable when in fact we found that no point source actually existed. Instead all of the final candidates were visually inspected to remove contaminated or false detections.

Our primary goal was the building of composite spectral energy distributions (SED) using archival data products. We initially considered *WISE* as the base catalog to astrometrically match with other data sets, but the *WISE* beam is significantly larger than other relevant all sky surveys. We also decided to use a near-IR band as a tracer of the stellar spectral type. Therefore we adopted the 2MASS (Skrutskie et al. 2006) catalog and coordinates as the base catalog. Requiring our sources to have a 2MASS companion reduced the size of our sample to 48,692.

## 2.1. Additional ancillary data

The Perseus star forming region is well covered by many large sky surveys (see Figure 1) from infrared to X-ray including: 2MASS, UKIRT Infrared Deep Sky Survey (UKIDSS), *Spitzer* (e.g., c2d, Evans et al. (2003)), the InfraRed Imaging Surveyor (AKARI) (Murakami et al. 2007), Sloan Digital Sky Survey (SDSS, DR8+), the AAVSO Photometric All-Sky Survey (APASS, Release 7)<sup>1</sup>, Chandra X-Ray Observatory and X-ray Multi-Mirror Mission (XMM-Newton) as well as catalogs based on older scanned photographic plates (US Naval Observatory: USNO-B1, UCAC3) and the USNO-B1/2MASS re-reduction, PPMXL (Roeser et al. 2010).

SDSS and APASS catalog measurements are adopted at optical wavelengths if available; otherwise, we have used PPMXL cataloged photometry for B and R bands. Figure 2 presents APASS and SDSS coverage of our surveyed region, showing how APASS provided nearly complete, deep optical coverage. While PPMXL covers the entire area, it is intrinsically based on USNO-b1 and contains much larger errors than APASS. Because PPMXL contains corrected positions, proper motions and optical-infrared matches of stars, we used it to break degeneracies for multiple matches between different catalogs. X-ray observations were very concentrated toward the known star forming regions, and did not cover

---

<sup>1</sup><http://www.aavso.org/apass>

the entire region. We benefited from archival X-ray data in publications to identify known YSOs. Because of its limited spatial scope (Figure 1) we neglected the UKIDSS catalog entirely. AKARI flux measurements were consistent with IRAC and MIPS observations, but only a few of our candidates had high quality AKARI data, therefore this catalog was not used in final SED fitting.

There are several narrow field catalogs at different wavebands in Perseus region, but to keep a high degree of uniformity in source detection and flux calibration we do not account for such observations. We further downloaded all SIMBAD sources in the survey area to identify previously known YSOs or census contaminating sources such as planetary nebulae, background galaxies or other type of known evolved stars.

We employed the *CDS X-match* Service <sup>2</sup> to match different catalogs and investigate the astrometric uncertainties. This service employs the coordinate errors to calculate the probability density of two sources from two different catalogs. The probability density is given by convolution between two Gaussian distributions around each source Pineau et al. (2011). We consider a completeness of 99.7 % at  $3\sigma$  criterion (only 0.3% of the counterparts could be missed).

### 3. IDENTIFYING DISK CANDIDATES

We adopt the shape of the spectral energy distribution (SED) to identify sources with excess infrared emission as these are probable young stars with passively reradiating circumstellar disks (Lada 1987). Following on the *Spitzer* based SED analysis of Lada et al. (2006) and Muench et al. (2007), we used a simple power-law, least-squares fit of the 3 – 12  $\mu\text{m}$  portion of the YSO’s SEDs as traced by the W1, W2, and W3 *WISE* bands (3.4, 4.6 and 12  $\mu\text{m}$ , respectively).

While Muench et al. (2007) showed that the *Spitzer* 3 – 8  $\mu\text{m}$  index was relatively insensitive to extinction, we acknowledge that including 12 microns into the SED slope fit will result in larger intrinsic dispersions in the slope distribution because of variations in the silicate feature. Unreddened classical T-Tauri stars with *SiO*<sub>4</sub> in emission will have very large slopes. We do not anticipate silicate absorption due to  $A_V$  to “remove” a source from our sample, by lowering the measured 3 – 12 micron slope.

Figure 3 presents a comparison between IRAC  $\alpha_{3-8}$  and WISE  $\alpha_{3-12}$  for 135 sources which have both data set in our sample. Solid line shows a least square fit (with slope of  $0.92 \pm 0.2$ , excluding three data points at right bottom corner with poor IRAC photometry) and dashed line presents equal values. There is a large scatter due to different wavelength, band width for each wavelength, beam size and sensitivity for Spitzer and WISE. A selection bias is involved as well. In Figure 3 all IRAC data is included if available, but only *WISE* with SNR>7 sources are selected in our initial sample. In general for  $\alpha_{3-8} < -2$ , we have found larger slopes for WISE  $\alpha_{3-12}$ , where anemic disks and stars are located (discussed further in section 3.3). IRAC and *WISE* slopes are not expected to match completely, for this reason we are not reporting classification for individual objects based on categories defined in Muench et al. (2007).

---

<sup>2</sup><http://cdsxmatch.u-strasbg.fr/xmatch>, Strasbourg Astronomical Data Center

The  $22\ \mu\text{m}$  was not considered in the initial slope-fit for two reasons: a) to keep detection uniformity for sources which have not been detected or have very low SNR in W4 and b) to avoid the overestimation of slopes due to poor sensitivity of W4 for faint sources with  $W4 > 8$ . However  $22\ \mu\text{m}$  flux, when regarded as real, is considered in final complete SED modeling to study the disk characteristics.

In the first attempt we filtered candidates based on *WISE* flags. We found a few strong YSO candidates which were located nearby saturated stars or within nebulous regions, had been flagged as poor detection or photometry due to contamination. On the other hand in visual inspection we found sources with very poor detection in cloudy areas which had high S/N fluxes reported with *WISE* high photometry quality flags but they did not survive our visual or point source profile inspections. Finally we decided to ignore the *WISE* flags at this stage and reconsider them after manual inspection.

We considered all sources with  $S/N > 7$  in first 3 *WISE* bands in our candidate pool and fitted a power-law to each source. Figure 4 shows the calculated slopes versus 2MASS  $J$  magnitude for 48,692 sources with  $S/N > 7$  in first 3 *WISE* bands in grey dots. To select the sources with excess emission we looked at the slope distributions in bins of 0.5  $J$  magnitude and fitted a Gaussian to the slopes distribution within each interval.  $J$  band is the shortest wavelength that we have uniform data for, and is thus the least contaminated wavelength by circumstellar disk emission, which makes it the best tracer of photospheric luminosity.

The selection criteria can be considered to be a convolution of variation in the intrinsic (photospheric) color as a function of apparent magnitude and the *WISE* sensitivity function. We did not consider disentangling these two functions as a useful exercise, and instead posited all sources with an excess greater than 5 sigma from the typical color as evidence for infrared excess.

The black locus in Figure 4 shows a  $5\sigma$  limit above the peak of distribution for each bin. All sources above the locus have significant excess in slope (and hence in IR emission) and are considered as candidates with excess. On average the slope increases with the  $J_{mag}$  after magnitude 12. Fainter objects in  $J$  band are either embedded sources, or background galaxies. Hence, faint YSOs are missed in this selection, but in return the final sample is less contaminated with background galaxies.

The  $J_{mag}$  error is not considered in calculating the locus, but it will not dramatically change the results. The maximum error in  $J_{mag}$  in our entire data set is only 1.7%. The locus has been drawn based on  $5\sigma$  above the mean population in each  $J_{mag}$  bin which means a confidence of 99.999943% of IR excess. Considering the largest error for  $J_{mag}$  around the locus, selected candidates are still more than  $4\sigma$  above the mean, which translates into a 99.994% confidence in IR excess. Therefore by neglecting  $J_{mag}$  error in our selection procedure we are not maintaining the  $5\sigma$  confidence for all selected YSO candidates, but all of the selected candidates have statistically significant IR excess.

669 sources met this criteria. However we are aware that the sample may contain none-stellar objects, contamination and false detections. In next step we filter candidate by manually inspecting them in optical and infrared images.

### 3.1. Visual inspection

*WISE* and 2MASS and if available SDSS images of each candidate which passed the locus selection were manually inspected. Visual inspection revealed that half of the selected sources cannot be considered resolved point sources. The first group were rejected as being identified as extended objects like galaxies and the second portion could not be identified as distinguished point sources in nebulous regions in a combination of at least any three *WISE* bands. We performed the eye inspection in three rounds and categorized the sources as contaminated, saturated, extended and not resolved. All extended objects were identified as galaxies and PNe in further investigations and were rejected. Candidates that could not be resolved as point sources in at least any three *WISE* bands needed to be inspected for the luminosity profile. Contaminated, saturated and not resolved sources were accepted and back to the list if they were resolved in 2MASS and if luminosity profile presented a point source in at least three *WISE* bands.

354 out of 669 candidates survived the visual inspection. These final candidates are presented by open red circles (new candidates) and blue triangles (known candidates) in Figure 4. The known AGB stars are presented with black dots. The sources in our list which are less likely to be YSOs and closer to the AGB stars are noted by black crosses. They are separated from the YSO candidates employing magnitude diagrams and will be discussed in more details in section 4. The known OB stars are also shown as yellow dots. The only OB star which is above the locus is *BD + 30540*. Rebull et al. (2007) identified this YSO as a class I source in their *Spitzer* c2d survey. It is a B8V star and have an estimated mass of  $2.6 M_{\odot}$ .

Figure 5 presents the spatial distribution of 354 final candidates on a *WISE* multi-color image. The brightness of each source is proportional to the the W1-3 slope; sources with larger slopes, which presumably have stronger disks, appear brighter in Figure 5.

### 3.2. Comparing classification schemes

Rebull et al. (2011) identified new YSO candidates in Taurus-Auriga region using preliminary *WISE* data. Nearly 25% of our survey area is covered in their study, therefore we looked for common candidates to evaluate our detection method accuracy. Rebull et al. (2011) report 94 new YSO candidates in Taurus-Auriga region, 22 of which lie within our survey area. Astrometry and photometry of more than 25% of sources have changed in *WISE* all-sky release, especially for bright sources in our list. Therefore preliminary and all sky release *WISE* catalogs do not contain identical IDs for all sources. Instead of matching IDs we performed a position match. Some photometries in the new *WISE* catalog also have slightly changed, but they are consistent enough with the preliminarily data to help selecting the right match. Rebull et al. catalog is plotted over our selection diagram in Figure 6. Our complete catalog of 354 sources are shown in black triangles. Rebull et al. known YSOs are shown with green dots and their new YSO candidates are shown with blue dots. They have also rejected many sources (shown in magenta dots) after various inspections. We have identified only 8 of Rebull’s new YSO candidates in our field. 14 unidentified sources are almost fainter than 12 magnitude in 2MASS *J* band and despite color excess they lie below our selection criteria.

We also have 17 of Rebull’s *known* candidates in our field. 14 have been classified as YSO candidates in our sample, one does not have 2MASS match and therefore not selected in our sample and two are below our selection criteria.

Rebull et al. also have 129 rejected candidates in our field which passed their color cuts in first place. 82 of their rejected sources (as background galaxies) match with our initial sample but lie below our selection criteria. 35 do not have 2MASS point source match and therefore not selected in our list. We have 8 common sources in our visually rejected list which they have identified as confused, galaxy, PNe or foreground/background star. Noticeably 7 of their rejected sources do not have a match in new WISE within  $1''$ , and 4 do not have a match within  $2''$ , therefore we cannot comment about these sources.

### 3.3. Comparing with color-cuts

We compared our candidates with the color-cut spaces described by Koenig et al. (2012). The color cuts are defined in multiple color spaces based on known different types of YSOs and other contaminant objects such as AGNs, galaxies with PAH-feature emissions and shock emission blobs. Koenig et al. (2012) selections are employing the results from *Spitzer* surveys to identify various objects with color excess (Gutermuth et al. 2009; Rebull et al. 2010) based on where they statistically lie on *WISE* + *2MASS* color-color spaces. Similar to  $\alpha$  selection technique, color-cut criteria in general can be adjusted to extract weaker disks with smaller IR excess or exclude them. In this section we compare our results with criteria defined by Koenig et al. (2012) which is frequently adopted in similar studies.

Following Koenig et al. (2012), no AGNs were identified in our sample of candidates, but three sources (J03504369+3507088, J04022740+3057450, J03504333+3346024) might be considered as PAH emitting/star forming galaxies. These objects have no match in the literature. They are out of the *Spitzer* field and not covered by SDSS, therefore their identity cannot be determined by the spectrum. It worths to mention that Koenig color-cuts are defined based on the *WISE* preliminary data, while photometry of 25% of sources have had slight changes in all sky release. That may partially affect their selection criteria at the borders.

Koenig et al. (2012) also used color-cuts to categorize their YSOs into different class types. Muench et al. (2007) (appendix A) explored the influence of dust extinction on  $\alpha$  detection technique and presented that IRAC SED slope for a diskless K0 star requires  $A_V > 100$  to inflect into a positive slope and even  $A_V > 200$  cannot inflect  $\alpha_{5.8-24}$  of background stars into positive. Such large column densities within typical molecular clouds occur only in protosellar envelop of embedded YSOs. But smaller values of dust extinction also may affect  $\alpha$  at the classification of ClassI/ClassII candidates. In contrast mid-IR color cut techniques can be defined such that they minimize extinction-induced bias. The goal of this study is only identifying YSOs and not classifying them. We present the classification only to compare the slope-fitting and the color cut methods and will not report the class types for our final candidates.

According to Muench et al. (2007),  $\alpha_{IRAC3-8} = -2.66$  corresponds to the predicted slope of M0 star photosphere. Accepting a typical precision of SED fits, they characterized sources with  $-2.56 < \alpha < -1.80$  as “anemic disks”. Transitions disks, disks with inner holes and heavily depleted

optically thin disks may locate in this category. Objects with  $\alpha_{IRAC3-8} < -2.56$  are considered stars, and objects with  $\alpha_{IRAC3-8} > -1.80$  are accepted as IR excess objects ( $-1.80 < \alpha_{IRAC3-8} < -0.5$  as Class II and  $-0.5 < \alpha_{IRAC3-8}$  as Class I).

Figure 7 compares the disk classification by Muench et al. (2007) based on the slopes ( $\alpha$ ) and Koenig color cuts in one plot. Grey dots show all 48,692 *WISE* sources in our field with  $\text{SNR} > 7$  for first three *WISE* bands. Black dots are  $\alpha$ -stars. Yellow dots show  $\alpha$ -anemic disks. Blue dots present Class II and red dots present Class I  $\alpha$ -disks. Based on Koenig classifications, green open circles present Class II and black open squares present Class I sources (selected in  $[3.4] - [4.6]$  and  $[4.6] - [12]$  color-color diagrams). There is a good agreement in disk identification type between two methods. However, color-cuts select less Class I protostars and many  $\alpha$ -Class I sources are identified as Class II by color-cuts.

We should remind that  $\alpha$  selection fails to detect faint sources ( $J_{mag} > 12$ ) even if they have noticeable color excess. On the other hand color-cut method misses the weak or evolved disks, even if they are bright sources. For example anemic disks have rarely been distinguished by color-cuts. The comparison between the selected YSOs in Rebull et al. (2011) and this work in Figure 6 also presents how the faint sources even with strong disks have been missed in  $\alpha$  selection, and how the bright sources with weak disks have been missed by color-cut selection. We suggest that to have a complete sample of faint to bright and weak to strong disks, both methods needed to be considered.

To summarize, we establish our working sample of candidate young stellar objects as selected by the spectral energy distribution power-law slope in range of  $3.4 - 12 \mu\text{m}$  from *WISE* all sky point source catalog. Using this method we can identify the weak and more evolved circumstellar disks if they are hosted by a bright protostar. These type of disks are barely identified with color-color diagrams. In contrast  $\alpha_{3-12}$  selection miss fainter sources, in particular those with  $J_{mag} > 12$  sometimes even if they have strong disks. Color-color diagrams are capable to select many fainter sources but the results are contaminated ( $\sim 67\%$  for example, in Rebull’s primary selected sources) with background galaxies and other fake detections compared to  $\alpha$  selection method. For example in pool of 1014 potential YSOs identified by Rebull et al. (2011), 686 were rejected as known galaxies or objects to be likely background galaxies in their final list.

## 4. CANDIDATE ANALYSIS

### 4.1. Known YSOs

We cross matched our candidates with the SIMBAD database to identify known YSOs and possible contaminants. Among 354 candidates passed our manual inspection as resolved point sources, J035523.11+310245.0 is a known massive X-ray binary and was removed. 12 other sources are known AGBs, Mira variables or other type of known evolved stars. 76 have matches with previously known YSOs or T-tau stars while 80 others are listed as YSO or T-tau candidates in SIMBAD. All these sources are categorized as known YSOs in our final catalog and listed in Table 3. 185 sources remain in our list as new YSO candidates, but 66 of them identified to be more likely evolved dusty stars and were separated from final new YSO candidates list (Table 4. We will discuss them in section 4.2.



Finally 119 sources survived as new YSO candidates in our final catalog and they are listed in Table 2. The errors (range of Lower limit and upper limit for each parameters) are provided in online tables.

#### 4.2. Dusty evolved stars

We checked the distribution of our sample in various color and magnitude diagrams to look for possible category and grouping objects. In particular  $22\ \mu\text{m}$  is the best indicator to probe the embedded objects. Figure 8 shows 2MASS  $K_{mag}$  plotted vs. *WISE*  $22\ \mu\text{m}$  for all 353 point sources (J035523.11+310245.0, the known massive X-ray binary is removed). It was noticeable that sources are divided into two main populations. Sources with the same W4 magnitude are divided into two brightness branches in  $K_{mag}$ . The lower group are usually bright stars with smaller slopes but they have statistically significant excess emission in longer wavelengths compared to main sequence stars. Known YSOs and YSO candidates lie in the upper group, with larger K magnitudes. Extreme brightness in  $K_{mag}$  of the lower population suggests that they can be dusty evolved stars. The majority of them are out of Perseus cloud and have low extinctions.

To characterize this “lower population” we compared them with the known AGB stars in our sample and in the literature. Grey dots in Figure 8 present all *WISE* sources in our survey field with  $\text{SNR} > 7$  for all four bands which mostly contain main sequence stars. Then we matched all known evolved stars in the Galaxy (including AGB stars, carbon stars and Mira variables) from SIMBAD with *WISE* catalog. Cyan dots show evolved stars which have a *WISE* match with  $\text{SNR} > 10$  in all four bands and we call it AGB branch in our diagram. The AGB branch in this plot is above the main sequence and perfectly matches with the “lower population”. 10 of the known evolved stars in our sample also lie in this area. We selected 66 objects from the “lower population” in K–W4 diagram as *dusty evolved star* candidates. These objects are shown by black crosses in Figure 8 left panel. Right panel in Figure 8 presents the K and M type stars in our sample which had known spectral type in the literature. While the majority of them locate within known and candidate YSOs, a smaller population lie within the AGB branch, indicating these objects are most likely evolved dusty stars rather than YSOs.

In addition we checked our AGB candidate with Blum et al. (2006) color-magnitude diagrams from their Large Magellanic Cloud *Spitzer* survey. In Figures 3 – 6 of their paper they present the location of carbon stars and extreme AGB stars on  $[3.6]$  vs.  $J-[3.6]$ ,  $[8]$  vs.  $J-[8]$ ,  $[3.6]$  vs.  $[3.6]-[8]$  and  $[24]$  vs.  $[8]-[24]$ . We replaced  $[3.6]$  by W1 ( $3.4\ \mu\text{m}$ ),  $[8]$  by W3 ( $12\ \mu\text{m}$ ), and  $[24]$  by W4 ( $22\ \mu\text{m}$ ) and applied their criteria. Although the wave bands are slightly different, our 66 AGB candidates reasonably matches the AGB stars criteria on their various plots. These candidates are listed in Table 4.

We also did a statistical estimation of how many AGB stars we expect to identify in our field. A recent *WISE* study (Tu & Wang 2013) estimated 470,000 of AGB stars in the Galaxy with contamination uncertainty of 20% of other sources including YSOs. Jackson et al. (2002) estimated a total of 200,000 AGB stars in the Galaxy. Using their volume density around solar neighborhood and integrating over 10 kpc (distance at which we can detect bright AGBs in our sample) we expect to have 100-400 AGB stars in our field. Therefore 66 likely AGB candidates plus 12 known evolved stars

in our field seems a reasonable number.

### 4.3. Spatial Distribution

Figure 9 presents the location of known and new YSO candidates, known and new candidate AGB stars and OB stars in  $12^\circ \times 12^\circ$  Per OB2 field. All the known YSOs (blue triangles) and the majority of new YSO candidates (red circles) are located within the nebulous region, bright in green color in Figure 5. New YSO candidates in North-East corner of the field follow the shell like dust feature and a large number of new YSOs in North-West side, toward the California nebula, are located where the remaining of the original Perseus cloud forms dense filamentary structures.

OB stars and known AGBs are shown in yellow and black dots respectively. Black crosses present our AGB candidates discussed above. These candidates are expected to be foreground/background sources, therefore we expect them to be randomly distributed in the field. Figure 9 does not confirm a random distribution. AGB candidates shown with crosses are following the cloud structure and also concentrated in North-West. Some of AGBs also might be below our locus and not selected in our sample. Therefore we suggest that a fraction of these objects might be YSOs with inaccurate photometry or at the border of contamination with AGBs.

## 5. MODELING SPECTRAL ENERGY DISTRIBUTION

A common procedure to find the spectral energy distribution model that better reproduces data is using  $\chi^2$  minimization: comparing a grid of models to the data points, finding the  $\chi^2$  value using the measurement errors, and picking the model that minimizes the  $\chi^2$  (e.g. Robitaille et al. (2007)). We call this solution the “Best Fit” model. However, besides the Best Fit solution, there might be many other models that have slightly larger  $\chi^2$  but that are also a reasonable solution for our fitting problem. If we consider the distribution of various physical parameters from all models with  $\chi^2$  smaller than a certain threshold, the peak of such distribution may not occur at the value given by the Best Fit. In other words, the Best Fit solution might not be located in the region of the parameter space where more models are a good representation of our data. Alternatively, we can assume that the model parameters are random variables, then derive probability distribution functions (PDFs) for them given our data, and find the parameter values that maximize those PDFs. In this paper we call the latter solutions the “Peak” values for the parameters, and we will use a Bayesian method to find them.

### 5.1. Bayesian approach

In Bayesian inference, the model parameters are considered as random variables for which posterior probability distributions can be derived from the likelihood of the solutions (that we obtain from the data and the measurement errors) and the parameter priors, where we encode the prior knowledge in these parameters before any data has been taken. Once we derive the posterior PDFs, we can draw samples from them in order to visualize the solution and find the absolute PDF maximum for each

parameter. An efficient way to perform this sample is by using a Markov Chain Monte Carlo (MCMC) method that randomly steps across the parameter space and at each iteration decides whether to accept the step based on an acceptance probability that depends on the ratio of probabilities between the current position and the proposed new position. This approach is particularly useful for multivariate problems like the one at hand here.

Our Bayesian algorithm is very similar to the implementation of the CHIBURST code for fitting SEDs of star-forming systems (Martínez-Galarza et al. 2014). Here we will describe only the aspects of the code that are relevant for the present work. As a model grid, we use the SED models of Robitaille et al. (2006), that have calculated the radiative transfer for the emission from the YSO as it traverses the disk and/or envelope that surrounds it. Synthetic SEDs are produced for a broad range of stellar masses ( $0.1 - 50M_{\odot}$ ), ages ( $10^3$ - $10^7$  yr), as well as disk and envelope sizes and geometries. Given a set of photometry and assuming this model grid is a fair description of the actual distribution of physical parameters in YSOs, we attempt to find the probability that a particular model represents the properties of the observed YSO.

This allows us to explore the inherent degeneracies that arise when we attempt to fit a limited amount of photometric data with a multivariate model. By solving for the PDF rather than just finding solutions listed by increasing  $\chi^2$ , we are able to visualize all the likely solutions for a particular object photometry, given the observational uncertainties and assuming that the parameter space of the model grid is a fair universal sample of the population of YSOs in the Perseus cloud. We focus on the determination of three main model parameters, namely the YSO stellar mass ( $m_*$ ), age ( $t_*$ ), and  $A_V$  in the line of sight towards our objects. To some extent, all other model parameters are determined by the selection of mass and age, or difficult to constrain without unavailable photometric bands.

### 5.1.1. The Probability Distribution Functions

Suppose that we have obtained photometry data (D) of a YSO at different bands, with certain observational uncertainties associated. Given our data, we can calculate  $P(\Theta|D)$ , the posterior PDF for the set of parameters  $\Theta$  as the product of the likelihood  $P(D|\Theta)$  and the prior  $P(M)$ . In the case of normally distributed measurement errors, the likelihood  $P(D|\Theta)$  can be obtained from the distribution of reduced  $\chi^2$  values:

$$P(D|\Theta) = \sum \exp(-1/2 \chi_{\text{red}}^2) \quad (1)$$

where the sum is marginalized for each model parameter over all possible models with a given value of the parameter. The *prior*  $P(M)$  is a measure of any previous knowledge that we have on a particular parameter or set of parameters. For example, if we have reliable extinction measurements in the line of sight towards a particular YSO, then we can constrain the possible solutions to our problem by constructing a prior on ( $A_V$ ) that is compatible with those extinction measurements. Finally, we need to apply a normalization factor to our posterior PDF to guarantee that the probability of at least one model being a representation for our YSO equals one.

### 5.1.2. Priors

We are mostly interested in obtaining a distribution of masses, evolutionary stages and optical extinctions for a sample of newly identified YSOs in the Perseus region. For the mass and age of the YSOs we have adopted the flat, uniform priors already set by the model grid, with boundaries set by  $0.1 M_{\odot} < M_{*} < 50 M_{\odot}$  and  $10^3 \text{ yr} < t_{*} < 10^7 \text{ yr}$ . We also chose a flat, uniform prior for the disk inclination, since we expect most of the inclination effects to cancel out for a sample of many YSO models. We must emphasize here that these priors are discreet (i.e., not all possible values of mass, age and inclination are possible), but we consider that the sampling is such that any uncertainty due to sampling is smaller than the uncertainties imposed by the observational errors and the model degeneracies. Most of the other priors (disk and envelope mass, accretion rate, etc.) are set by the mass and age of a particular YSO, and have been thoroughly explained in (Robitaille et al. 2006). We adopt a distance of 320 kpc to the Perseus molecular cloud, but allow for a random scaling of the model YSOs to account for a distance uncertainty of 25%. We also obscure the models and characterize this obscuration by an  $A_V$  value, to account for any foreground extinction in the line of sight towards the Perseus cloud. We construct the prior on  $A_V$  using an extinction map produced by Lombardi et al. (2010). The prior is simple: we restrict the possible values of  $A_V$  to be within 0.4 dex of the value obtained from the extinction map. We will later modify this prior to show the effect of the  $A_V$  on determining the mass of the YSOs.

### 5.1.3. Stepping across the parameter space

Calculating the posterior PDF at every single point of the model grid and for all possible values of distance scaling and  $A_V$  would be computationally time consuming, specially as more data points are added and additional model parameters (i.e. multiplicity of YSOs) are considered. Instead, we use a Monte Carlo Markov Chain (MCMC) approach to draw samples from the posterior PDF across the multidimensional space of parameters  $\Theta$ . We use the Metropolis algorithm with a uniform transition probability for the Markov Chain (i.e., given our current position in the parameter space, it is equally probable moving in any direction). After enough iterations of the MCMC, the histogram of model parameters in our chain should be a good representation of the posterior PDF. It is from this final histogram that we select the “Peak” solutions for our parameters.

## 5.2. Examples

Figure 10 shows the best fits and associated posterior PDFs for several types of SEDs found in Perseus sample. The method is quite successful at finding solutions for almost all types of SEDs. More importantly, the plotted PDFs show the usefulness of the method in determining the uniqueness of the solution.

It is important to realize the meaning of the best fit value as compared to the most likely solution as represented by the peak of the posterior PDF. They do not always coincide, which should not be surprising. The reason is that the best fit can be located in a region of the parameter space where not too many models agree with the data. The value obtained from the peak of the PDF, on the

other hand, provides the most likely value for a given parameter given all possible combinations of a parameter value with all the other parameters, constrained by the information contained in the priors. In a sense, the posterior PDF is a full description of all possible solutions. This is a significant improvement over the listing of the ten best fitting models, since these can be all located very near the best fit value, but not necessarily include the peak of the PDF. Furthermore, as we will see later, bimodal solutions are also possible due to degeneracies between the parameters, and usually the 10 best fitting models all fall near one of the two possible solutions to the problem.

### 5.2.1. Degeneracies

Degeneracy is a common issue of all data-fitting problems that more than one combination of model parameters give a reasonable solution within the observational uncertainties. This problem of model degeneracies has been particularly neglected in the case of YSO SED fitting, partly because of the lack of enough data to break those degeneracies, but also due to a blind faith on the “best fit” solution, even for objects with only a few photometric observations. Our method allows to clearly visualize the degeneracies between model parameters and hence it helps us consider other possible solutions that might be hidden in the complexity of our multi-parametrical model, and that might be in better agreement with independent determinations of the parameters. It also allows us to explore how those degeneracies behave as a function of the priors, i.e., how additional information or additional data points can break these degeneracies.

Figures 11 and 12 shows an example of model degeneracies. Shown are two different realizations of the fit to the source J03284618+3116385. Two groups of solutions are possible, one with low foreground extinction ( $A_V < 1$ ) and a low stellar mass, and one with higher  $A_V$  and higher mass. Physically, this can be understood as a need for a higher stellar mass to produce the same UV and optical flux when more obscuration is at work. In the unconstrained case shown in the figure, both fits are equally satisfying, but the solution with small  $A_V$  appears as more likely. Notice that the PDF for age remains unchanged. This implies that there is a strong degeneracy between stellar mass and extinction when fitting multi-wavelength SEDs of YSOs. Without a better prior for the  $A_V$  (or the stellar mass), we might choose the low mass-solution, but additional evidence could make the other solution more likely. For example, if we know that the  $A_V$  has to be greater than 1, then the low mass solution has to be neglected. This degeneracy is observed in many of the SEDs, in particular those of class IIa YSOs, as classified by (Gutermuth et al. 2009). Figure 13 shows the same effect much more clearly in the 2D  $m_*$ - $A_V$  plane. The choice of a particular  $A_V$  determines the estimated mass of the YSO.

In fact, rather than thinking in terms of a “best fit”, we should think in terms of likelihood of a solution given certain constrains on the values and all possible combinations of parameters.

It is possible to modify the prior on  $A_V$  by considering independent determinations of the physical conditions. We have obtained extinction values from the maps produced by Lombardi et al. (2010) and constrained the  $A_V$  prior accordingly. Since the extinction map have their own uncertainties, we allow our  $A_V$  values to vary within 0.4 dex of the value obtained from the maps. By doing so, we hope to break the degeneracy observed in Figure 13 for at least some of the objects. It is important

to notice here that the values of  $A_V$  measured from the map represent in fact only an upper limit to the total extinction, since part of the measured  $A_V$  can actually be coming from behind the source of interest. By selecting a range of values around the measured  $A_V$ , we are assuming that most of the extinction we see is due to foreground material between us and the source. Figure 13 shows the solution and the resulting marginalized posterior PDFs after the prior has been modified as described, for the same object of Figures 11 and 12. As expected, the additional information of the prior breaks the existing degeneracy and leaves only the most massive of the two solutions. This solution is in fact in better agreement with the expected mass for YSOs that we would be able to detect at the distance to the Perseus cloud. Of course, another way to break degeneracies might be by including additional data-points at longer wavelengths that are compatible with only one of the two possible solutions. Photometry from the PACS instrument onboard the Herschel Space Observatory will be instrumental for this task.

### 5.3. Results and discussion

#### 5.3.1. SED slope analysis

We have applied our SED fitting method to 275 identified YSOs (total of known and new candidates) in order to perform a census of masses and evolutionary stages. The calculated parameters are highly dependent on the extinction, and therefore we had to estimate the dust absorptions in order to constrain  $A_V$  before the SED fitting was applied. The extinction values are calculated based on 2MASS K band extinction map provided by Lombardi et al. (2010). Figure 15 presents the location of high ( $A_V > 2$ ) and low ( $A_V < 2$ ) extinction regions. Currently active star forming regions such as NGC 1333, IC 348, L1448, L1455 and Taurus all are embedded within Perseus molecular clouds and have higher extinctions.

Figure 16 presents the distribution of calculated  $\alpha_{3.4-12}$  and position of candidates in three distinct groups. For the first group,  $\alpha_{3.4-12}$  peaks at  $\approx -2$  and these sources are noted by blue circles in right panel for objects with  $\alpha_{3.4-12} < -1.75$ . This group have more evolved disks and are spread over the field with a concentration at North-West of the field, above the California nebula.

The main peak at  $\alpha_{3.4-12} \approx -1$  contains many YSOs with stronger disks. Green triangles present this group, selected as  $-1.75 < \alpha_{3.4-12} < 0$  in the right panel. They are more concentrated within the Perseus and Taurus star forming regions and molecular cloud.

Candidates with very strong disks are presented with red dots and are selected as  $0 < \alpha_{3.4-12}$ . They are highly concentrated within active star forming clusters, NGC1333, IC348, and Taurus with a few spread over the field. It is not clear if they are formed individually or escaped from their original birthplace.

Distinct population in Perseus region has been noted and discussed in several studies. For example Herbig (1998) found evidence of different generation of stars within and around IC348 cluster. Also suggested by a hipparcos study (de Zeeuw et al. (1999) and references therein), and later confirmed by Belikov et al. (2002) Per OB2 contains two kinematically separated subgroups. Belikov et al. (2002) identified more than 800 members for Per OB2 within a 50 pc diameter. We also have identified three

separated evolutionary stages which will be discussed more in next section.

### 5.3.2. Parameters from SED fitting

Using the Bayesian MCMC method described, we have obtained best fit and peak values for all the YSOs in our sample. We focus on the peak values for stellar mass, age, total luminosity and extinction. Given the limited amount of information at wavelengths longer than  $22 \mu\text{m}$ , we do not attempt to constrain the disk/envelope properties with accurate details. Instead, we are interested in studying the distribution of masses and ages in our wide select field that includes NGC 1333 and IC 348, as well as another less dense concentration of YSOs located near California nebula.

We should note that the derived parameters using Robitaille et al. (2007) models are “model-dependent-fit parameters” and not physical values. The YSO grid of models are randomly sampled in mass and age, and then use evolutionary tracks from Siess et al. (2000) to calculate all the other stellar properties. This means that the “age” derived here is not measured with respect to any physical stellar process, such as the start of deuterium burning. Rather, the reported ages are indications of the relative evolutionary stages of the members which are dependent on model assumptions and priors.

Willis et al. (2013) found a noticeable difference in total mass of their large complete sample of YSOs in NGC6334, derived from the same set of models used in this paper, compared to the expected total mass for a complete Kroupa IMF. Robitaille models employed in this study are simulated based on observation and physical parameters, therefore results are valid as a relative ratio of the evolutionary stage of all sources in the survey that satisfies the goal of this study.

Figure 14 shows the age probability vs. mass probability for 2MASS J03311069+3049405. The blue cross which presents the best fit is very close to the most probable models for both mass and age in left panel. In some cases, however, the best fit model is very different from the probability peak. 2MASS 03253790+3108207 (right panel) is a good example where *Best Fit* and *Peak Value* do not match well. There are two main reasons for this mismatch: first, the PDFs plotted here are marginalized versions of the PDFs, and are therefore integrated over all other parameters not shown in the plot. It is therefore likely that the absolute maximum of the multi-dimensional PDF does not always coincide with the maximum of a marginal distribution. Also, degeneracies in the models, specially given the lack of far-IR data points, might produce multiple maxima in the probability distributions.

We also realized that the correct estimation of the optical extinction is very important to constrain the mass and other physical parameters. The fitting tool lets  $A_V$  to accept the values in a wide range, to find the best SED models. But not constraining  $A_V$  will dramatically affect the final results. We fixed this problem by constraining  $A_V$  from observed values of extinctions toward each individual candidate using the  $A_K$  value from the extinction map provided by Lombardi et al. (2010) toward Taurus and Perseus star forming regions, based on 2MASS counts. We have recorded the best fit values for the parameters for each source, as well as the most likely solution or the peak value as obtained from the peak of the posterior PDF.

Figure 17 presents the distribution of estimated ages for our candidates and the age spatial

distribution in the field. Three distinct age groups are noticeable in left histogram:  $\text{age} < 1 \text{ Myr}$ ,  $1 < \text{age} < 5 \text{ Myr}$  and  $5 \text{ Myr} < \text{age}$ . As expected, the younger YSOs are having stronger disks and locate within the high extinction inner parts of the Perseus cloud and NGC1333 and IC348 clusters. Noticeably the North-Western association do not contain any young YSOs and only a few mid-age ones.

The estimated masses for our YSO candidates varies in a wide range from  $0.1$  to  $5 M_{\odot}$ . Figure 18 presents the mass distribution and the location of low mass and high mass candidates. The majority of YSOs with masses larger than  $1 M_{\odot}$  are located within areas with larger  $A_V$ , i.e. within Perseus molecular cloud and particularly star-forming clusters. The massive YSOs from older populations spread over the field are probably too evolved to have strong, detectable disks.

## 6. summary

We have performed a census of YSO candidates in Perseus OB2 association covering  $\sim 144 \text{ deg}^2$  using *WISE* catalog. We derived physical characteristics of all identified YSOs within the region by employing other optical and infrared data including 2MASS, *Spitzer*, SDSS, PPMXL and APASS. Following Lada et al. (2006) Muench et al. (2007) we calculated the SED slope in range of  $3 - 12 \mu\text{m}$  for 48,692 sources which had a  $S/N \leq 7$  in first three *WISE* bands. 669 point sources survived to have slopes larger than the  $5\sigma$  above the peak in bins of  $0.5$  2MASS J magnitude. Removing known non-stellar extended objects such as galaxies and PNe we still had some sources remained in our sample that could not be identified as point sources in optical or infrared images or did not show point source profiles in at least three out of four *WISE* bands. Among 354 remained point sources one was identified as a massive X-ray binary and 12 as evolved stars such as carbon stars or Mira variables. 156 of remained sources were previously identified as YSO or YSO candidates. In this work we present 119 new YSO candidate toward the Perseus region. We also identified 66 new point sources with infrared excess emission but brighter than normal YSOs in the region. We separated them as likely AGB and evolved star candidates.

The majority of known candidates are concentrated toward active star forming regions such as Taurus, IC348 and NGC1333 clusters. We add more YSO candidates in these regions which had poor photometry in *c2d* or other previous studies to be confirmed as YSOs. New candidates also follow the remaining gas of the original Perseus cloud with a concentration toward North-West near California nebula. In total, new candidates have weaker disks and are more scattered within the field, while previously known sources locate within high  $A_V$  regions in Perseus molecular cloud.

We employed the SED fitting models described by Robitaille et al. (2007), but used a Markov Chain Monte Carlo method to explore the large parameter space of the model grid. Instead of selecting the model with the lowest  $\chi^2$  solution as the best fit, we accept the physical parameters from the most probable fitted models. Similar to the slope ( $\alpha_{3.4-12}$ ) distribution, derived mass and ages also present separated populations.  $\alpha_{3.4-12}$  histogram shows two separated peaks at  $\approx -2$  and  $\approx -1$ . Candidates with slopes larger than zero (i.e. very strong disks) are mainly found within IC348 and NGC1333 clusters with a few scattered in the field. The mid-slope population which peaks around  $-1$  are also located within the Perseus cloud and nebulous region.



As expected, younger sources (age < 1 Myr) are located within active star forming clusters while older population (age > 5 Myr) are scattered within the field with a noticeable concentration toward North-West. In contrast both low mass ( $M < 1 M_{\odot}$ ) and higher mass ( $M > 1 M_{\odot}$ ) candidates are found equally scattered within the field or located within the Perseus cloud.

Finally, we compared our method of selecting circumstellar disks with other YSO selecting methods based on optical and infrared color and magnitudes. While our  $\alpha$  method is very successful to identify bright sources with weak disks that will be filtered in other methods, our method misses YSOs with strong disks if they are faint and in particular fainter than  $J_{mag} = 12$ . A combination of both  $\alpha$  and color-cut selection would be a complete method to identify both strong and weak disks.

### **Acknowledgment**

We thank Matthew Templeton for providing us with APASS data and Marco Lombardi and Joao Alves for sharing Taurus-Perseus  $A_K$  map based on their 2MASS study. We also would like to thank Luisa Rebull for helpful discussion and comments and the anonymous referee for detailed comments and suggestions that helped to improve this work. This publication makes use of data products from the Wide-field Infrared Survey Explorer, which is a joint project of the University of California, Los Angeles, and the JPL/California Institute of Technology, funded by NASA. This publication makes use of data products from the Two Micron All Sky Survey, which is a joint project of the University of Massachusetts and the Infrared Processing and Analysis Center/California Institute of Technology, funded by NASA and NSF. This research has made use of the NASA/ IPAC Infrared Science Archive, which is operated by JPL, California Institute of Technology, under contract with NASA. This research was made possible through the use of the AAVSO Photometric All-Sky Survey (APASS), funded by the Robert Martin Ayers Sciences Fund. This research has made use of the SIMBAD database and X-Match tool, operated at CDS, Strasbourg, France. This research funded by the National Aeronautics and Space Administration Grants NNX08AJ66G, NNX10AD68G, NNX12AI55G, and JPL RSA 717352 to the Smithsonian Astrophysical Observatory.

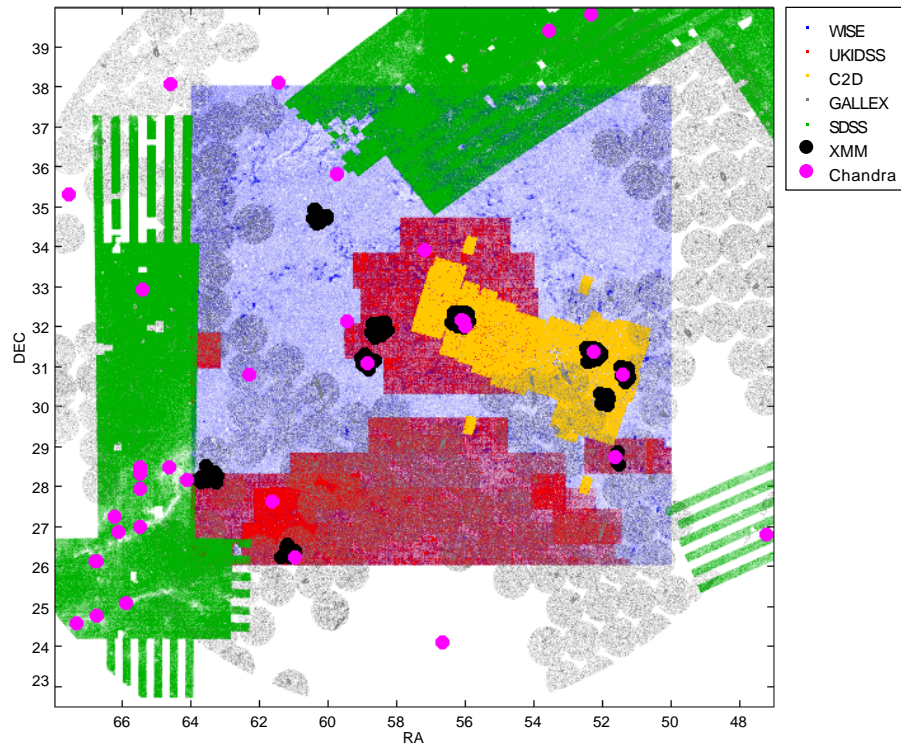


Fig. 1.— Surveyed Region and its coverage by a sample of surveys: WISE (blue), Spitzer (c2d) (yellow), SDSS (green), UKIDSS (red), Gallex (grey), XMM (black) and Chandra (magenta).

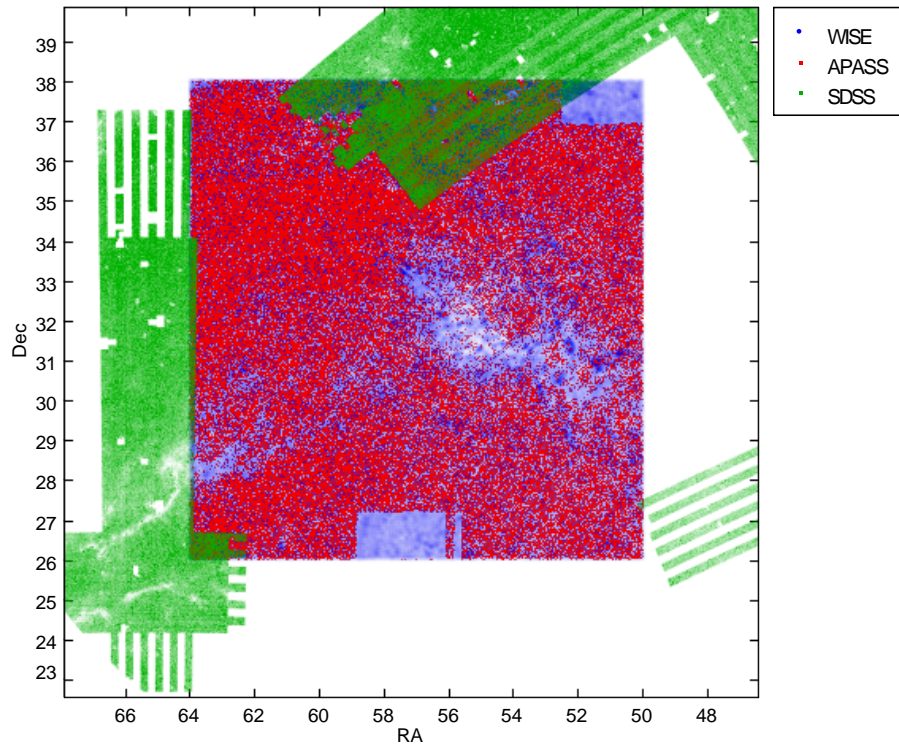


Fig. 2.— Field coverage by SDSS, APASS and WISE

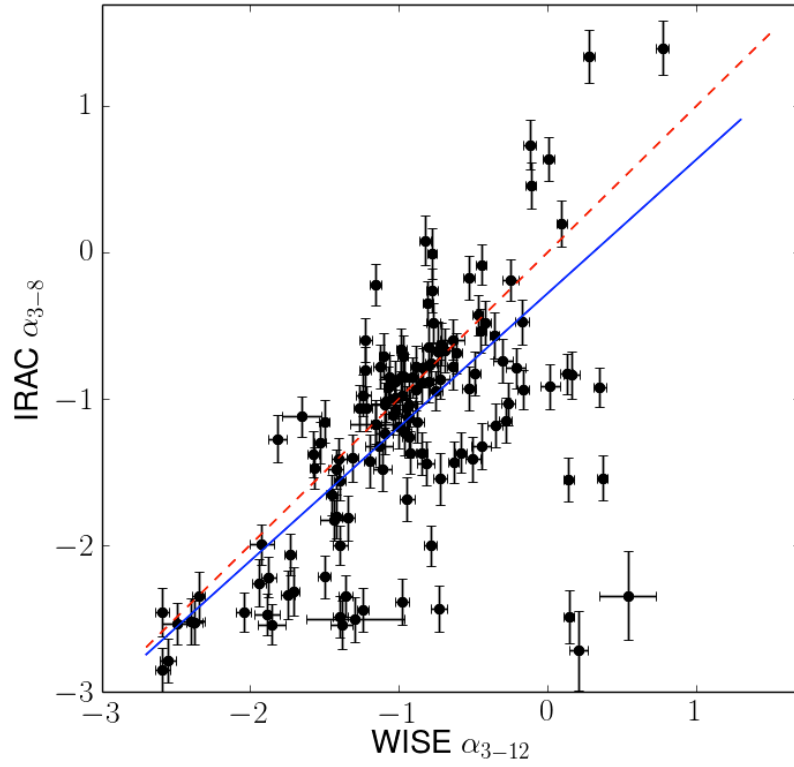


Fig. 3.— IRAC  $\alpha_{3-8}$  vs. WISE  $\alpha_{3-12}$ . Solid blue line presents a linear least square fit with slope of  $0.92 \pm 0.2$  (excluding three data points at right bottom corner with poor IRAC photometry) and red dashed line presents equal values.

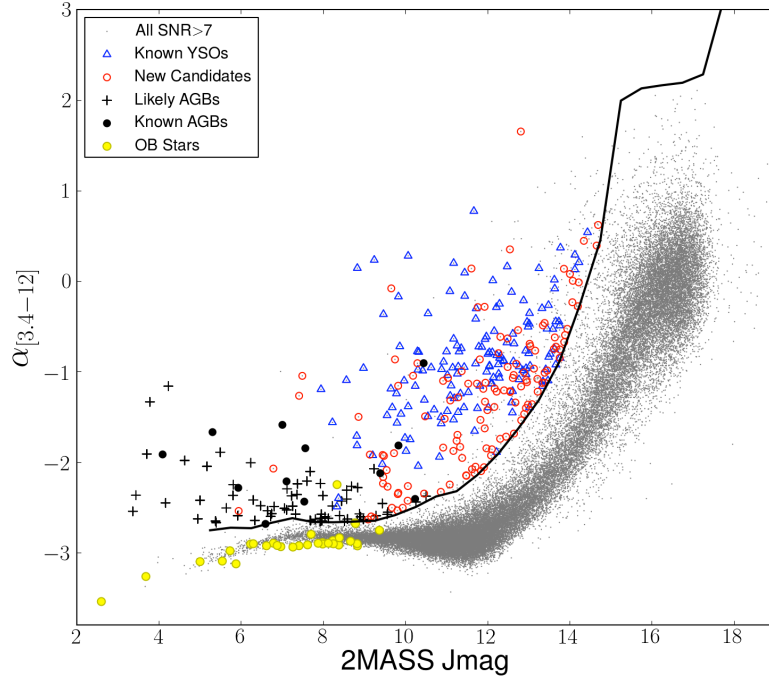


Fig. 4.—  $\alpha_{3.4-12}$  versus 2MASS J magnitude were used to identify the YSO candidates. Grey dots show all *WISE* point sources with  $\text{SNR} > 7$  in first three bands. Black locus separates sources with  $\alpha_{3.4-12}$  which are  $5\sigma$  above the Gaussian peak of slope distribution in each  $J_{mag}$  0.5 magnitude bins. New identified YSO candidates are presented with open red circles while known candidates from literature are shown in blue triangles. Known AGB stars are presented in black bold dots in this plot while AGB candidates identified in this study are presented in black crosses. Yellow dots present OB stars in Per OB2.

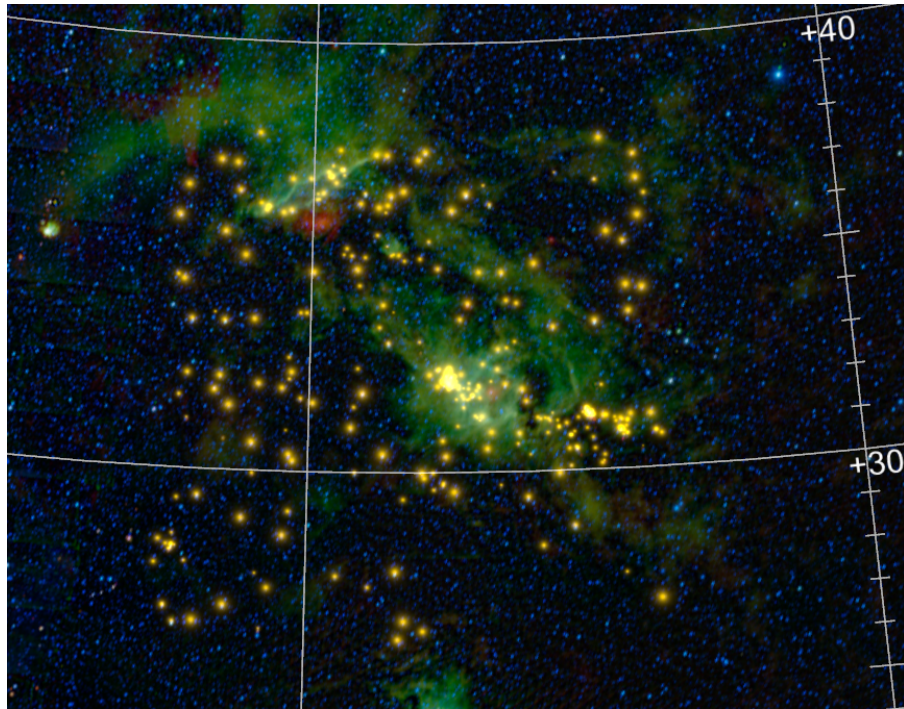


Fig. 5.— YSO candidates overlaid on multi band WISE image of Perseus region ( $4.6\mu\text{m}$  in blue,  $12\mu\text{m}$  in green and  $22\mu\text{m}$  in red). The brightness of each source presents its  $\alpha_{3.4-12}$  slope. Larger slope presumably means stronger disks. Picture created using Microsoft Worldwide Telescope (<http://worldwidetelescope.org>)

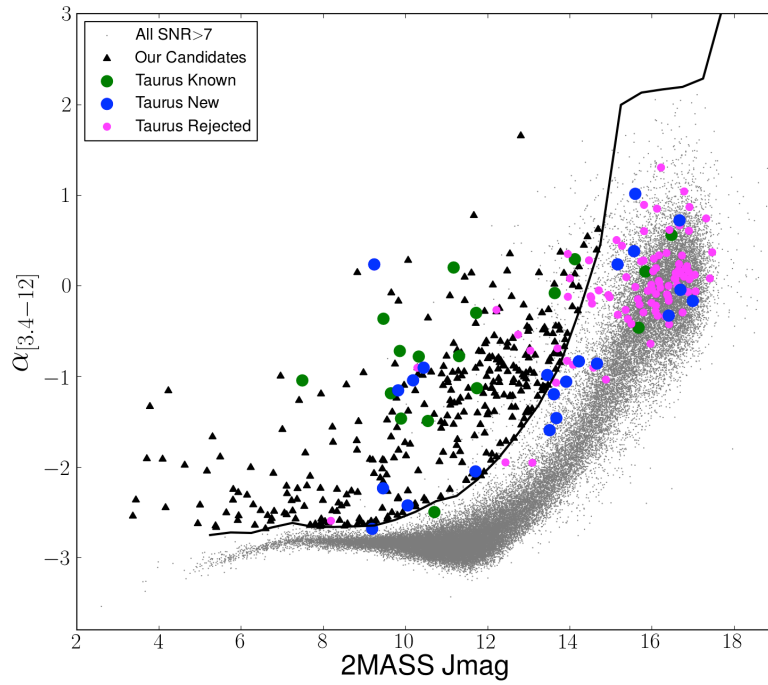


Fig. 6.— Comparing our results with Rebull et al. (2011) study of Taurus-Auriga star forming region. Black triangles present our sample of 354 candidates in Perseus. Green, blue and pink dots presents known YSO candidates, new YSO candidates and rejected candidates respectively from Rebull et.al.

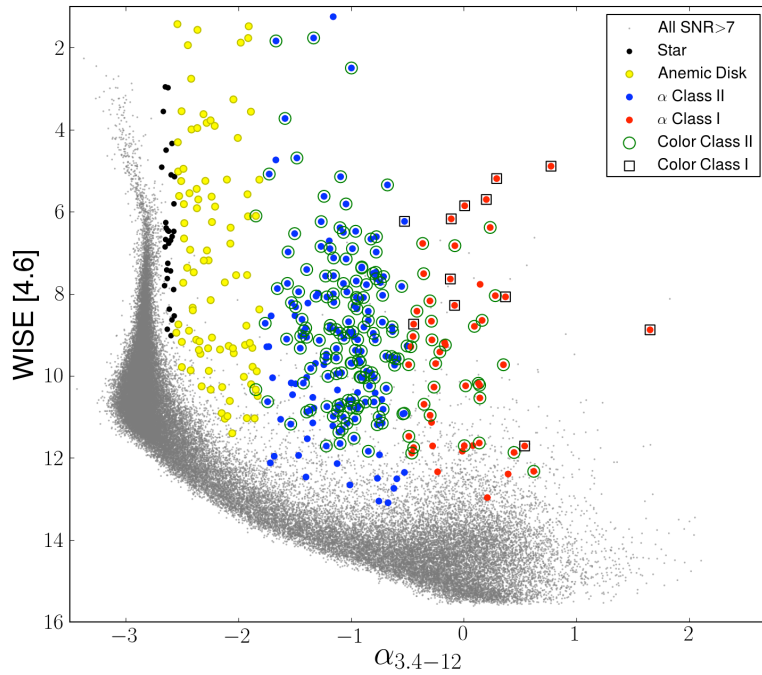


Fig. 7.— Comparing disk classification based on the slopes ( $\alpha$ ) and Koenig color cuts in one plot. Black dots show  $\alpha$ -stars ( $\alpha < -2.56$ ) and yellow dots show  $\alpha$ -anemic disks ( $-2.56 < \alpha < -1.8$ ). Blue dots show Class II ( $-1.8 < \alpha < -0.5$ ) and red dots present Class I  $\alpha$ -disks ( $\alpha > -0.5$ ). Selected by  $[3.4] - [4.6]$  and  $[4.6] - [12]$  color-color diagrams, green open circles present Class II and black open squares present Class I sources.



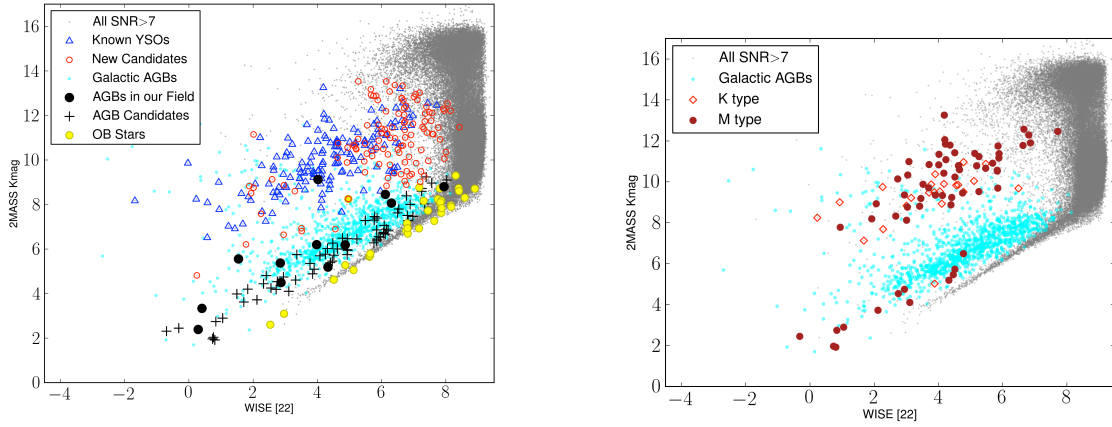


Fig. 8.— Left: our candidate with infrared excess are divided into two groups. The brighter sources with brighter  $K_{mag}$  match with known Galactic AGB stars (cyan dots) in this plot and are likely AGB stars and not YSOs. They are noted with black crosses. Right: M and K type stars in our sample similarly follow the same pattern, empowering the suggestion that sources noted by cross in left panel are likely M and K type evolved dusty stars.

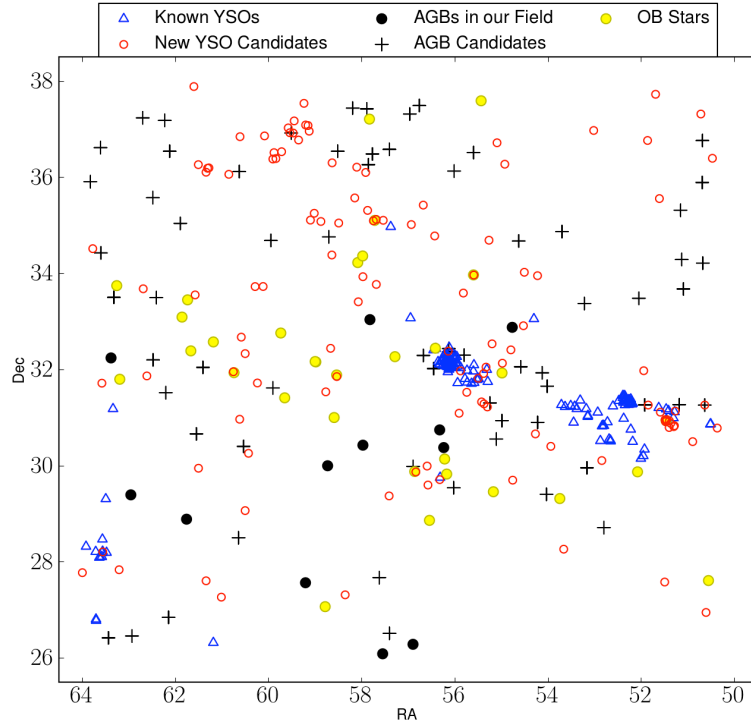


Fig. 9.— Distribution of YSO, AGB and OB stars in Per OB2. As expected YSOs are concentrated toward star forming clusters (IC348, NGC1333) and more numerous within the Perseus molecular cloud. AGB candidates are expected to be randomly distributed in the field but they are following the cloud structure and also concentrated in North and North-West of the field.

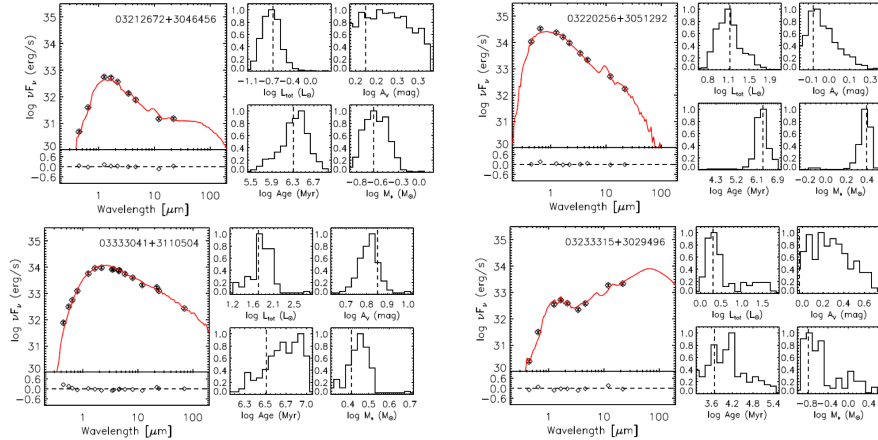


Fig. 10.— Multi-wavelength SEDs for a selection of objects in Perseus. The black diamonds are the extracted photometry, while the red line is the best fit (the one that minimizes the  $\chi^2$ ). Also shown are the posterior PDFs for  $m_*$ ,  $t_*$ ,  $L_{\text{tot}}$  and  $A_V$ , with the best fit values represented by the dotted lines.

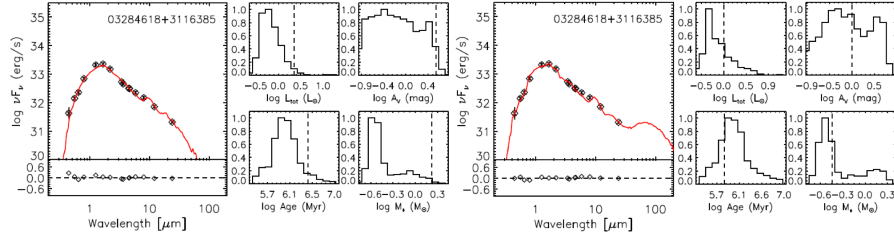


Fig. 11.— The  $m_*$ - $A_V$  degeneracy. Two possible solutions for a single set of photometry. The PDFs show the two possible solutions, while the best fit in each case tends to select only one.

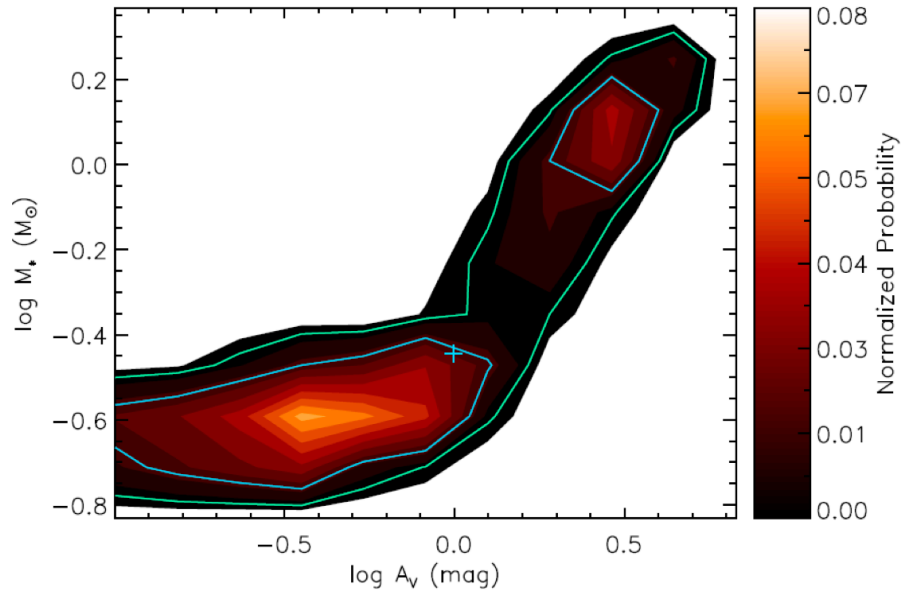


Fig. 12.— The  $m_*$ - $A_V$  plane with contours of normalized probability showing the degeneracy between these two model parameters. The blue cross indicates the best fit for this particular realization.

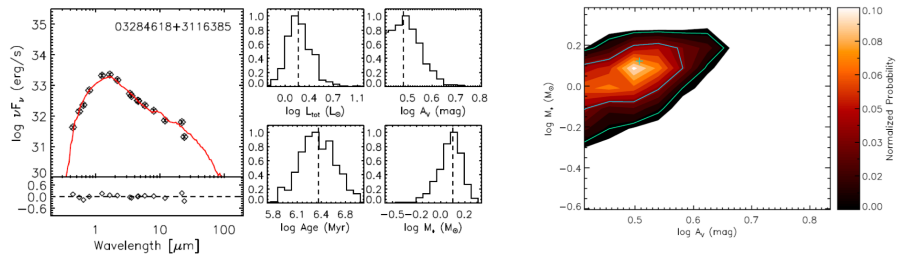


Fig. 13.— Only one solution is possible when the  $A_V$  prior is modified to account for additional evidence on the extinction.

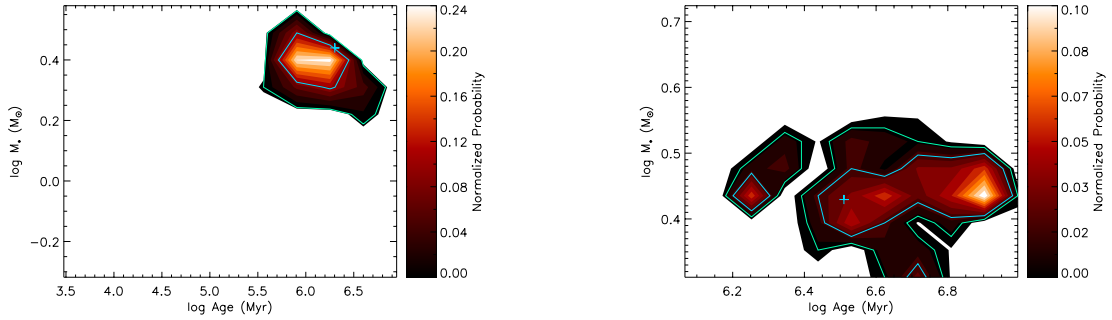


Fig. 14.— Mass-Age probability distribution for all fitted SED models for two different YSO candidates. The brightest region presents the most probable values from different fitted SED models. In the right panel the best-fit values (blue cross) is close to the most probable values but in the right panel there is a large difference.

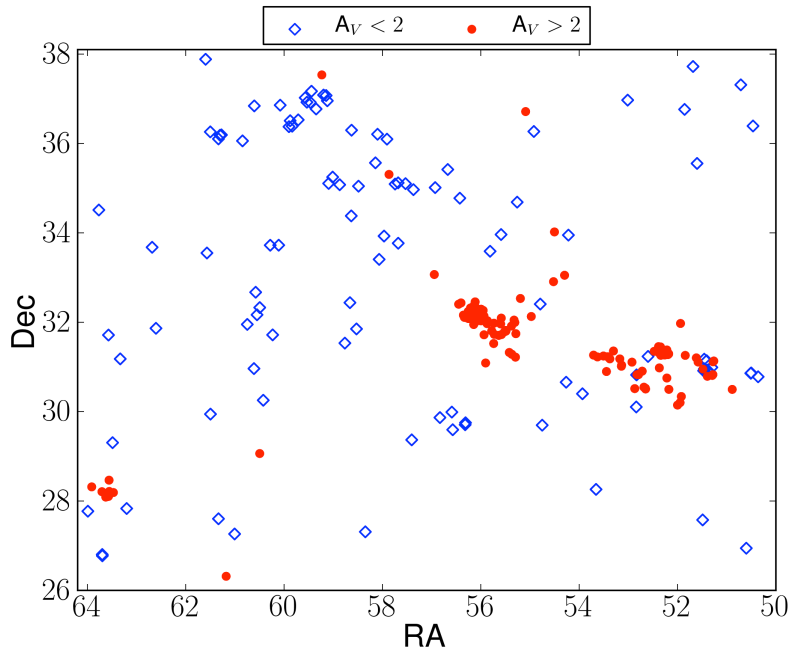


Fig. 15.— Spatial distribution of extinction for 275 YSO candidates.  $A_V$ s are calculated based on 2MASS K band extinction map by Lombardi et al.

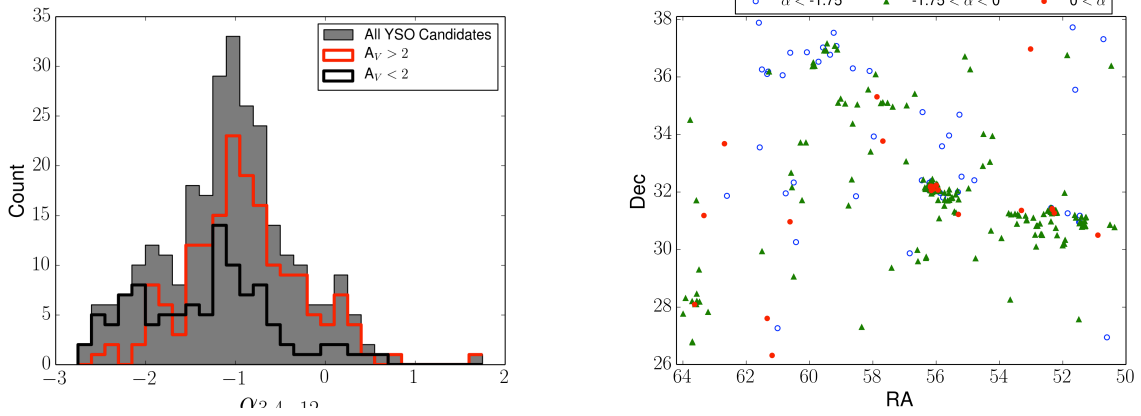


Fig. 16.— Distribution of  $\alpha_{3.4-12}$  for 275 YSO candidates. The location of members of three noticeable groups are shown in right panel.  $\alpha < -1.75$  in blue circles,  $-1.75 < \alpha < 0$  in green triangles and  $0 < \alpha$  in red dots.

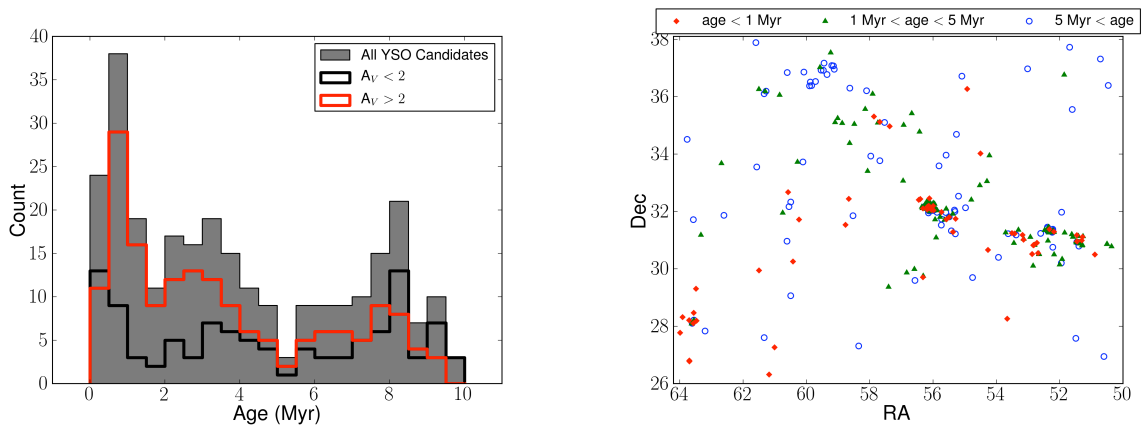


Fig. 17.— Age distribution for 275 YSO candidates. The location of members of three noticeable groups are shown in right panel.  $\text{age} < 1$  Myr in red dots,  $1 < \text{age} < 5$  Myr in green triangles and  $5 < \text{age}$  in blue circles.

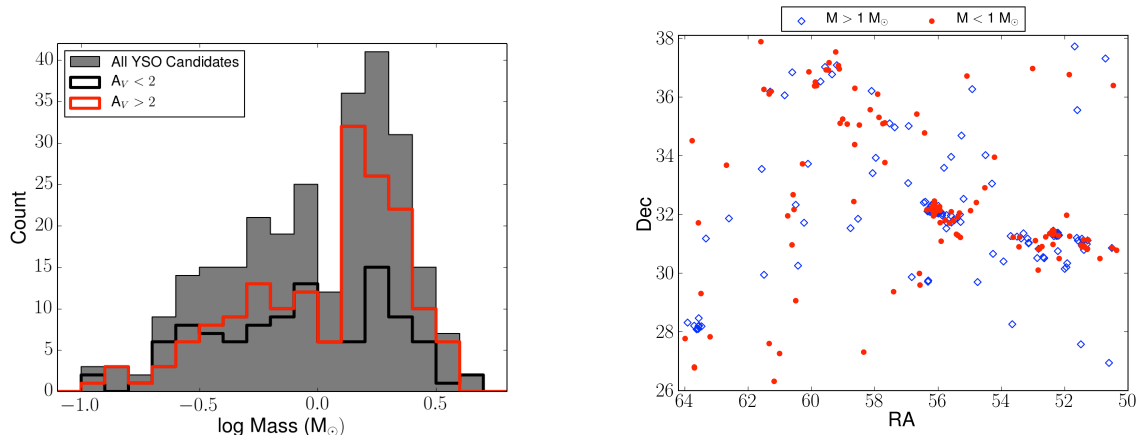


Fig. 18.— Mass distribution for 275 YSO candidates. The location of two noticeable groups are shown in right panel.  $M < 1 M_{\odot}$  in red dots and  $M > 1 M_{\odot}$  in blue squares.

## REFERENCES

- Arce, H. G., Borkin, M. A., Goodman, A. A., Pineda, J. E., & Halle, M. W. 2010, *ApJ*, 715, 1170
- Bally, J., Walawender, J., Johnstone, D., Kirk, H., & Goodman, A. 2008, *The Perseus Cloud*, ed. B. Reipurth, 308
- Belikov, A. N., Kharchenko, N. V., Piskunov, A. E., et al. 2002, *A&A*, 384, 145
- Blum, R. D., Mould, J. R., Olsen, K. A., et al. 2006, *AJ*, 132, 2034
- de Zeeuw, P. T., Hoogerwerf, R., de Bruijne, J. H. J., Brown, A. G. A., & Blaauw, A. 1999, *AJ*, 117, 354
- Enoch, M. L., Evans, II, N. J., Sargent, A. I., & Glenn, J. 2009, *ApJ*, 692, 973
- Evans, II, N. J., Allen, L. E., Blake, G. A., et al. 2003, *PASP*, 115, 965
- Gutermuth, R. A., Megeath, S. T., Myers, P. C., et al. 2009, *ApJS*, 184, 18
- Herbig, G. H. 1998, *ApJ*, 497, 736
- Jackson, T., Ivezić, Ž., & Knapp, G. R. 2002, *MNRAS*, 337, 749
- Jørgensen, J. K., Harvey, P. M., Evans, II, N. J., et al. 2006, *ApJ*, 645, 1246
- Kirk, H., Johnstone, D., & Di Francesco, J. 2006, *ApJ*, 646, 1009
- Koenig, X. P., Leisawitz, D. T., Benford, D. J., et al. 2012, *ApJ*, 744, 130
- Lada, C. J. 1987, in *IAU Symposium, Vol. 115, Star Forming Regions*, ed. M. Peimbert & J. Jugaku, 1–17
- Lada, C. J., Muench, A. A., Luhman, K. L., et al. 2006, *AJ*, 131, 1574
- Lombardi, M., Lada, C. J., & Alves, J. 2010, *A&A*, 512, A67
- Martínez-Galarza, J. R., Smith, H. A., Lanz, L., et al. 2014, *ArXiv e-prints*, arXiv:1412.2760
- Muench, A. A., Lada, C. J., Luhman, K. L., Muzerolle, J., & Young, E. 2007, *AJ*, 134, 411
- Murakami, H., Baba, H., Barthel, P., et al. 2007, *PASJ*, 59, 369
- Pineau, F.-X., Motch, C., Carrera, F., et al. 2011, *A&A*, 527, A126

Table 1. Physical parameters measured for the entire sample

Catalog	Coverage Type	Coverage of $12^\circ \times 12^\circ$	Waveband	Number of Sources
2MASS	all sky	100%	J, H, K	887,729
WISE	all sky	100%	3.4, 4.6, 12, 22 $\mu\text{m}$	1,657,265
USNO-UCAC3	all sky	100%	579-642 nm	205,279
USNO-B1	all sky	100%	B, R, I	2,072,601
PPMXL	all sky	100%	B, R, I	833,291
NOMAD	all sky	100%	B, R, I	815,242
GSC	all sky	100%	J, V, N, U B	850,673
AKARI	all sky	100%	9, 18 $\mu\text{m}$	1399
SDSS DR8	selected regions	$\sim 10\%$	u, g, i, r, z	59,4967
UKIDSS DR7	selected regions	$\sim 50\%$	J,H,K,Y,Z	1,842,326
C2D-cloud	selected regions	$\sim 15\%$	3.6, 4.5, 5.8, 8.0, 24,70,160 $\mu\text{m}$	777484
C2D-off	selected regions	$\sim 2\%$	3.6, 4.5, 5.8, 8.0, 24,70,160 $\mu\text{m}$	55,193
Chandra	selected regions	$< 2\%$	0.3-3 $\text{\AA}$	887
XMM-Newton	selected regions	$< 2\%$	0.6-6 $\text{\AA}$	819



Table 2. Physical parameters measured for the 119 new candidates

Order	Catalog Number	RA (deg)	Dec (deg)	Name	$\alpha$	$M_{\text{MassBF}}$ ( $M_{\odot}$ )	$M_{\text{Masspeak}}$ ( $M_{\odot}$ )	$\text{Age}_{\text{BF}}$ (Myr)	$\text{Age}_{\text{peak}}$ (Myr)
1	J032126.73+304645.5	50.3613824	30.7793282		-1.74 ± 0.05	0.2	0.35 ± 0.07	0.56	3.06 ± 0.23
2	J032151.66+362327.7	50.4652808	36.3910322		-1.39 ± 0.05	1.42	0.93 ± 0.22	9.67	9.32 ± 0.13
3	J032224.49+265637.9	50.602025	26.943878	BD+26 545	-2.63 ± 0.04	1.97	1.86 ± 0.06	9.79	8.35 ± 0.1
4	J032231.00+311527.2	50.629184	31.25754		2.62 ± 0.04	2.54	2.8 ± 0.0	1.04	1.12 ± 0.0
5	J032251.21+371842.7	50.713394	37.3118834		-2.25 ± 0.06	1.16	1.15 ± 0.22	4.53	5.85 ± 0.23
6	J032333.14+302949.8	50.8881155	30.4971848	IRAS 03204+3019	1.65 ± 0.03	0.52	0.64 ± 0.32	0.03	0.03 ± 0.6
7	J032503.08+310755.9	51.2628556	31.1322201		-1.54 ± 0.05	0.23	0.38 ± 0.18	3.37	3.41 ± 0.46
8	J032507.48+304941.9	51.2811739	30.8283286		-1.07 ± 0.05	0.33	0.46 ± 0.16	2.42	3.82 ± 0.26
9	J032510.59+304834.7	51.2941413	30.8096523		-1.08 ± 0.05	0.24	0.39 ± 0.33	4.18	3.53 ± 0.26
10	J032526.49+305237.4	51.3604161	30.877062		-1.04 ± 0.04	0.66	0.35 ± 0.61	8.02	3.55 ± 0.25
11	J032533.16+305544.1	51.3881758	30.9289289		-1.19 ± 0.04	0.2	0.3 ± 0.09	0.38	1.12 ± 0.31
12	J032534.52+304728.0	51.3938412	30.7911121		-0.69 ± 0.04	1.29	1.46 ± 0.21	3.3	8.81 ± 0.25
13	J032546.87+305720.4	51.4453023	30.9556944	2MASS J03254686+3057204	-0.61 ± 0.04	1.38	1.39 ± 0.37	0.05	0.04 ± 0.61
14	J032550.10+305554.1	51.4587901	30.9317144	BD+30 540	-2.25 ± 0.05	2.49	2.63 ± 0.17	4.34	6.15 ± 0.19
15	J032552.76+305449.0	51.469849	30.9136219	2MASS J03255275+3054490	-1.53 ± 0.05	0.65	0.5 ± 0.11	2.63	2.8 ± 0.2
16	J032555.72+305705.4	51.4822053	30.9515063		-1.88 ± 0.05	1.06	0.89 ± 0.1	4.61	3.31 ± 0.22
17	J032557.49+273436.3	51.4895635	27.5767754		-0.29 ± 0.04	1.5	1.19 ± 0.3	6.3	9.16 ± 0.16
18	J032619.81+310637.1	51.5825609	31.1103143		-1.19 ± 0.04	1.62	1.36 ± 0.06	2.84	1.03 ± 0.34
19	J032624.73+353310.1	51.603061	35.552788	HD 278643	-2.62 ± 0.04	2.07	2.03 ± 0.15	4.23	5.58 ± 0.35
20	J032644.45+374319.9	51.6852328	37.7221956	HD 275417	-2.5 ± 0.04	1.97	1.99 ± 0.29	9.79	9.03 ± 0.19
21	J032722.41+311528.7	51.8434013	31.2579774		-1.85 ± 0.05	0.42	0.56 ± 0.08	2.35	2.6 ± 0.28
22	J032725.66+364542.0	51.8569303	36.7616939		-1.22 ± 0.06	0.1	0.11 ± 0.3	2.44	4.81 ± 0.32
23	J032745.45+315821.0	51.9394058	31.9725183		-0.91 ± 0.04	0.85	0.95 ± 0.08	8.03	6.43 ± 0.16
24	J033121.45+300614.3	52.8393947	30.1039948		-1.12 ± 0.05	0.12	0.13 ± 0.11	2.3	2.87 ± 0.27
25	J033203.36+365810.0	53.0140256	36.9694462		0.45 ± 0.06	0.61	0.74 ± 0.38	5.27	9.59 ± 0.12
26	J033437.78+281536.8	53.6574328	28.2602328		-1.67 ± 0.06	1.46	1.5 ± 0.0	0.51	0.19 ± 0.0
27	J033544.16+302357.5	53.9340301	30.3993128		-0.01 ± 0.05	1.49	1.47 ± 0.11	3.03	5.7 ± 0.17
28	J033652.68+335658.0	54.2195016	33.9494472		-1.7 ± 0.05	0.65	0.79 ± 0.13	1.64	3.02 ± 0.24
29	J033703.64+303929.0	54.2651805	30.6580796	TYC 2355-740-1	-0.86 ± 0.03	1.27	1.94 ± 0.1	0.46	0.57 ± 0.11
30	J033800.72+340112.6	54.5030092	34.020184	2MASS J03380072+3401126	-1.73 ± 0.06	1.07	1.54 ± 0.0	0.27	0.29 ± 0.0
31	J033805.39+325428.5	54.5224599	32.9079195		-1.16 ± 0.07	0.62	0.47 ± 0.07	6.58	2.91 ± 0.3
32	J033900.55+294145.7	54.7523308	29.6960465	V* V1185 Tau	-0.08 ± 0.04	3.3	2.17 ± 0.21	4.35	7.95 ± 0.13
33	J033909.97+322421.8	54.7915742	32.4060745		-2.15 ± 0.08	0.76	0.85 ± 0.26	3.51	4.86 ± 0.23
34	J033941.31+361604.3	54.9221469	36.2678697	GSC 02367-01706	-1.0 ± 0.15	2.76	2.8 ± 0.0	0.1	0.11 ± 0.0
35	J033953.88+320742.6	54.9745076	32.1285048		-0.53 ± 0.07	1.25	0.3 ± 0.16	4.39	8.39 ± 0.22

Table 2—Continued

Order	Catalog Number	RA (deg)	Dec (deg)	Name	$\alpha$	Mass <sub>BF</sub> (M <sub>⊙</sub> )	Mass <sub>peak</sub> (M <sub>⊙</sub> )	Age <sub>BF</sub> (Myr)	Age <sub>peak</sub> (Myr)
36	J034021.42+364248.4	55.0892783	36.7134484		-0.28 ± 0.04	0.3	0.31 ± 0.11	8.02	7.9 ± 0.12
37	J034046.96+323153.7	55.1956827	32.5315911	V* IP Per	-1.92 ± 0.05	2.44	2.19 ± 0.04	6.73	5.39 ± 0.17
38	J034102.75+344111.8	55.2614645	34.686616	HD 278919	-2.27 ± 0.04	1.91	1.85 ± 0.3	8.85	7.29 ± 0.0
39	J034110.99+311308.0	55.2958295	31.2188936		0.0 ± 0.06	0.3	0.34 ± 0.03	8.02	7.83 ± 0.15
40	J034117.95+320250.9	55.3247937	32.0474798		-0.75 ± 0.06	0.21	0.29 ± 0.13	3.6	8.28 ± 0.26
41	J034128.70+311658.1	55.3695924	31.2828254		-0.23 ± 0.07	0.47	0.35 ± 0.21	0.22	0.4 ± 0.32
42	J034130.52+315452.3	55.3771731	31.9145545		-1.36 ± 0.05	0.18	0.72 ± 0.12	2.6	3.01 ± 0.3
43	J034141.12+311924.7	55.4213386	31.3235488		-1.34 ± 0.05	0.44	0.59 ± 0.06	6.21	6.88 ± 0.16
44	J034158.52+314855.7	55.4938374	31.8154967	SSTc2d J034158.6+314855	-1.07 ± 0.04	2.22	2.12 ± 0.22	9.89	8.46 ± 0.3
45	J034221.27+335743.5	55.5886603	33.9620971	BD+33 698B	-2.16 ± 0.05	1.91	1.89 ± 0.05	8.85	7.49 ± 0.0
46	J034257.36+313124.5	55.7390175	31.5234811		-1.33 ± 0.07	1.22	1.1 ± 0.21	6.66	5.42 ± 0.17
47	J034314.92+333516.1	55.8122066	33.5878064	HD 278934	-1.9 ± 0.04	2.29	2.21 ± 0.13	9.02	9.12 ± 0.1
48	J034329.67+315808.9	55.8736578	31.9691642		-1.86 ± 0.09	1.22	1.13 ± 0.23	9.86	7.41 ± 0.18
49	J034336.78+310516.5	55.9032525	31.0879277		-1.01 ± 0.04	0.54	0.45 ± 0.16	7.16	2.81 ± 0.38
50	J034432.72+322243.0	56.1363454	32.3786267		-2.35 ± 0.04	1.75	1.1 ± 0.12	1.48	1.69 ± 0.24
51	J034516.57+294224.4	56.319061	29.7067829		-1.28 ± 0.04	3.62	3.39 ± 0.12	0.0	0.0 ± 0.33
52	J034542.58+344631.9	56.42743	34.775547	NSV 1272	-1.76 ± 0.04	2.0	0.95 ± 0.11	0.7	2.31 ± 0.25
53	J034617.26+293540.6	56.5719328	29.5946356		-0.86 ± 0.04	0.99	0.79 ± 0.11	7.21	6.23 ± 0.21
54	J034621.58+295920.8	56.5899559	29.9891256		-1.36 ± 0.05	0.37	0.35 ± 0.13	6.07	4.13 ± 0.22
55	J034641.48+352502.0	56.6728344	35.4172376		-1.0 ± 0.03	1.01	0.81 ± 0.04	2.38	3.31 ± 0.27
56	J034719.71+295200.0	56.8321391	29.8666734	HD 281258	-1.93 ± 0.04	1.78	1.91 ± 0.08	7.63	3.5 ± 0.26
57	J034742.94+350044.1	56.9289537	35.0122731	NSV 1302	-1.1 ± 0.04	1.55	1.4 ± 0.15	5.9	3.59 ± 0.25
58	J034937.39+292205.2	57.4058169	29.368137		-1.12 ± 0.04	0.37	0.34 ± 0.09	3.61	3.65 ± 0.2
59	J035007.75+350603.3	57.5322953	35.1009271	GSC 02364-00805	-1.72 ± 0.07	1.42	1.01 ± 0.14	9.67	9.5 ± 0.11
60	J035043.33+334602.5	57.6805755	33.7673872		0.62 ± 0.04	0.24	0.24 ± 0.19	9.42	8.08 ± 0.3
61	J035043.70+350708.9	57.6820945	35.1191647		-0.6 ± 0.06	0.53	0.53 ± 0.17	0.04	0.04 ± 0.14
62	J035058.53+350528.5	57.7438986	35.0912715		-0.97 ± 0.05	0.13	0.25 ± 0.17	2.6	4.04 ± 0.22
63	J035128.19+351825.8	57.8674971	35.3071818		0.14 ± 0.04	0.46	0.5 ± 0.24	0.36	0.44 ± 0.36
64	J035138.16+360546.2	57.9090149	36.0961775		-0.49 ± 0.05	1.25	0.19 ± 0.0	4.39	4.0 ± 0.22
65	J035152.40+335541.1	57.9683514	33.9280997	HD 279119	-2.09 ± 0.04	1.91	1.88 ± 0.04	8.85	7.62 ± 0.0
66	J035216.28+332422.1	58.0678615	33.4061622	HD 279128	-1.27 ± 0.05	2.59	2.89 ± 0.04	2.71	2.1 ± 0.28
67	J035224.19+361221.4	58.1008192	36.2059517	HD 279075	-2.5 ± 0.05	1.91	1.77 ± 0.14	8.85	8.28 ± 0.25
68	J035234.42+353358.9	58.1434471	35.5663787		-1.12 ± 0.04	0.36	0.35 ± 0.24	4.49	2.27 ± 0.2
69	J035233.82+271838.3	58.3492848	27.310649		-0.99 ± 0.04	0.11	0.38 ± 0.14	7.59	6.91 ± 0.18
70	J035357.09+350239.2	58.4878805	35.0442238		-1.13 ± 0.04	1.87	0.69 ± 0.03	3.61	4.17 ± 0.3

Table 2—Continued

Order	Catalog Number	RA (deg)	Dec (deg)	Name	$\alpha$	Mass <sub>BF</sub> (M <sub>⊙</sub> )	Mass <sub>peak</sub> (M <sub>⊙</sub> )	Age <sub>BF</sub> (Myr)	Age <sub>peak</sub> (Myr)
71	J035407.02+315101.8	58.5292786	31.850522	BD+31 666E	-2.6 ± 0.04	1.91	1.97 ± 0.07	8.85	8.94 ± 0.13
72	J035431.06+361747.7	58.629428	36.2966037		-2.06 ± 0.07	1.17	0.91 ± 0.14	9.81	7.49 ± 0.17
73	J035432.45+342245.7	58.6352227	34.3793737		-1.22 ± 0.05	0.52	0.44 ± 0.1	5.17	4.55 ± 0.19
74	J035438.91+322616.8	58.6621312	32.4380016		-0.85 ± 0.05	0.25	0.27 ± 0.21	0.38	0.38 ± 0.31
75	J035503.75+313157.4	58.7656359	31.5326213		-0.91 ± 0.03	2.15	2.13 ± 0.09	7.32	0.91 ± 0.32
76	J035528.93+350435.5	58.8705711	35.0765338		-1.32 ± 0.04	0.75	0.72 ± 0.16	3.19	3.06 ± 0.24
77	J035603.22+351450.5	59.0134429	35.2473748		-1.22 ± 0.04	1.03	0.62 ± 0.18	0.77	3.02 ± 0.29
78	J035622.85+350618.5	59.0952433	35.1051579		-0.46 ± 0.05	0.12	0.21 ± 0.19	3.62	3.67 ± 0.24
79	J035629.21+365717.2	59.1217283	36.9547837		-0.75 ± 0.09	0.3	0.3 ± 0.1	8.02	9.6 ± 0.12
80	J035635.23+370421.2	59.1468169	37.0725814		-1.93 ± 0.07	0.79	0.75 ± 0.05	5.67	7.57 ± 0.13
81	J035647.69+370500.3	59.1987252	37.0834308		-1.52 ± 0.05	1.54	1.42 ± 0.11	7.1	7.9 ± 0.17
82	J035656.17+373202.1	59.2340637	37.5339431		-1.95 ± 0.04	0.57	0.91 ± 0.08	2.99	2.73 ± 0.22
83	J035723.92+364615.4	59.3496905	36.7709473		-2.15 ± 0.07	1.17	1.23 ± 0.13	6.97	8.79 ± 0.24
84	J035746.60+371006.7	59.4441938	37.1685303		-1.12 ± 0.07	0.46	0.31 ± 0.1	8.87	8.4 ± 0.15
85	J035751.71+365501.2	59.4654968	36.917001		-1.68 ± 0.09	0.86	0.61 ± 0.1	9.46	8.35 ± 0.11
86	J035808.98+365520.7	59.5374326	36.9224253		-0.62 ± 0.07	0.3	0.3 ± 0.12	8.02	7.72 ± 0.08
87	J035817.28+370120.5	59.5720174	37.0223663		-1.84 ± 0.05	0.62	1.07 ± 0.04	2.75	3.06 ± 0.24
88	J035851.36+363140.0	59.7140014	36.5277881	HD 279222	-2.34 ± 0.05	1.91	2.03 ± 0.22	8.85	8.3 ± 0.1
89	J035920.81+362308.0	59.836732	36.385564		-0.77 ± 0.07	0.38	0.82 ± 0.11	6.72	8.31 ± 0.11
90	J035930.57+363031.4	59.8773908	36.5087443		-0.67 ± 0.08	0.3	0.23 ± 0.19	8.02	8.53 ± 0.18
91	J035936.50+362231.5	59.9021105	36.3754322		-1.01 ± 0.07	0.77	0.67 ± 0.07	5.56	9.32 ± 0.17
92	J040019.35+365123.6	60.0806382	36.8565579		-2.12 ± 0.08	1.22	0.95 ± 0.04	9.86	8.25 ± 0.12
93	J040026.64+334326.5	60.1110131	33.7240537	HD 281352	-1.49 ± 0.04	1.54	1.59 ± 0.15	7.1	8.22 ± 0.11
94	J040056.13+314301.3	60.2338993	31.7170481	TYC 2357-1345-1	-1.16 ± 0.04	3.27	2.2 ± 0.28	0.44	0.49 ± 0.44
95	J040107.93+334320.9	60.2830825	33.7224846		-1.21 ± 0.04	1.13	0.55 ± 0.05	1.14	1.88 ± 0.33
96	J040141.98+301516.3	60.424928	30.2545303	V* WW Tau	-2.54 ± 0.09	4.24	4.1 ± 0.06	0.49	0.62 ± 0.2
97	J040159.15+321941.2	60.4964818	32.328137	HD 281479	-2.24 ± 0.04	1.81	1.92 ± 0.07	8.29	8.31 ± 0.35
98	J040159.27+290344.2	60.4969797	29.062297		-1.47 ± 0.06	1.29	0.76 ± 0.12	6.92	7.51 ± 0.0
99	J040219.09+324015.2	60.5795592	32.6709063		-0.8 ± 0.04	0.2	0.23 ± 0.05	0.92	0.63 ± 0.4
100	J040225.72+365025.4	60.6071825	36.8404101	HD 279280	-2.35 ± 0.04	1.96	2.02 ± 0.08	5.06	8.36 ± 0.34
101	J040227.39+305745.3	60.6141306	30.9625879		0.39 ± 0.04	0.24	0.3 ± 0.13	9.42	9.22 ± 0.05
102	J040259.96+315703.9	60.7498591	31.9510947		-2.05 ± 0.04	0.6	0.51 ± 0.11	0.31	2.23 ± 0.27
103	J040323.26+360327.2	60.8469493	36.0575797		-2.33 ± 0.06	1.36	1.36 ± 0.08	9.49	4.97 ± 0.2
104	J040401.78+271545.4	61.0074512	27.2626172	IRAS 04010+2707	-1.92 ± 0.05	0.81	0.78 ± 0.3	0.17	0.28 ± 0.21
105	J040506.06+361129.2	61.2752807	36.1914563		-1.63 ± 0.07	0.95	0.89 ± 0.13	7.92	6.9 ± 0.13

Table 2—Continued

Order	Catalog Number	RA (deg)	Dec (deg)	Name	$\alpha$	Mass <sub>BF</sub> (M <sub>⊙</sub> )	Mass <sub>peak</sub> (M <sub>⊙</sub> )	Age <sub>BF</sub> (Myr)	Age <sub>peak</sub> (Myr)
106	J040512.95+361102.9	61.3039635	36.1841551		-2.53 ± 0.06	1.28	1.04 ± 0.1	1.33	1.2 ± 0.25
107	J040520.46+273608.2	61.3352698	27.6022827	IRAS 04023+2728	0.08 ± 0.04	0.27	0.26 ± 0.1	6.18	6.04 ± 0.13
108	J040520.61+360605.0	61.3358901	36.1014137		-2.08 ± 0.06	0.65	0.81 ± 0.17	5.11	5.36 ± 0.2
109	J040559.62+295638.2	61.4984288	29.9439538		-1.05 ± 0.03	2.68	2.1 ± 0.07	0.37	0.52 ± 0.46
110	J040600.41+361531.6	61.5017086	36.2587885		-1.83 ± 0.05	1.22	0.87 ± 0.11	9.86	4.38 ± 0.17
111	J040616.84+333256.3	61.5701758	33.5489916	HD 281534	-2.26 ± 0.05	1.91	2.1 ± 0.08	8.85	7.58 ± 0.24
112	J040623.36+375259.9	61.597374	37.883377		-2.1 ± 0.06	1.04	0.92 ± 0.05	5.55	9.26 ± 0.18
113	J041025.61+315150.7	62.6067479	31.8640941	HD 281664	-2.43 ± 0.06	1.91	1.83 ± 0.15	8.85	7.21 ± 0.2
114	J041044.36+334036.1	62.6848703	33.6767131		0.14 ± 0.04	0.98	0.55 ± 0.13	2.17	3.04 ± 0.24
115	J041248.58+274956.2	63.2024526	27.832299	2MASS J04124858+2749563	-0.54 ± 0.04	0.33	0.46 ± 0.16	3.86	6.73 ± 0.11
116	J041412.92+281212.2	63.5538407	28.2033957	[CGI2005] 4	-1.05 ± 0.05	3.68	3.78 ± 0.09	1.47	1.21 ± 0.62
117	J041417.39+314247.7	63.5724876	31.7132503		-0.95 ± 0.04	0.51	0.41 ± 0.47	8.07	7.37 ± 0.22
118	J041504.40+343040.1	63.7683363	34.5111655		-1.4 ± 0.07	1.29	0.77 ± 0.34	6.92	8.29 ± 0.11
119	J041558.00+274617.1	63.9916924	27.7714435	2MASS J04155799+2746175	-1.13 ± 0.04	0.23	0.22 ± 0.0	0.39	0.39 ± 0.31

Table 3. Physical parameters measured for the 156 known candidates

Order	Catalog Number	RA (deg)	Dec (deg)	Name	$\alpha$	Mass <sub>BF</sub> ( $M_{\odot}$ )	Mass <sub>peak</sub> ( $M_{\odot}$ )	Age <sub>BF</sub> (Myr)	Age <sub>peak</sub> (Myr)
1	J032200.52+305153.1	50.5022079	30.8647526	2MASS J03220052+3051531	-1.45 ± 0.04	0.8	0.95 ± 0.05	1.53	1.3 ± 0.34
2	J032202.57+305129.3	50.5107177	30.8581628	2MASS J03220256+3051292	-1.56 ± 0.04	2.75	2.62 ± 0.04	2.01	2.13 ± 0.25
3	J032506.71+310652.9	51.2779972	31.1147102	2MASS J03250672+3106528	-1.4 ± 0.04	1.82	1.43 ± 0.23	0.72	0.52 ± 0.24
4	J032512.59+305921.9	51.3024683	30.9894241	2MASS J03251260+3059215	-1.16 ± 0.04	1.65	1.6 ± 0.21	1.06	0.63 ± 0.28
5	J032537.91+310820.9	51.407985	31.1391488	2MASS J03253790+3108207	-0.92 ± 0.04	0.55	0.95 ± 0.32	6.41	2.8 ± 0.26
6	J032548.90+305725.8	51.4537885	30.9571679	2MASS J03254886+3057258	-0.96 ± 0.04	1.49	1.61 ± 0.08	9.08	0.68 ± 0.4
7	J032549.83+311023.8	51.4576476	31.1732939	2MASS J03254982+3110237	-2.02 ± 0.04	3.24	1.79 ± 0.11	0.84	0.81 ± 0.36
8	J032628.22+311207.8	51.6175851	31.2021747	2MASS J03262821+3112078	-0.95 ± 0.03	2.04	1.77 ± 0.05	0.44	1.92 ± 0.4
9	J032741.48+302016.8	51.9228373	30.3380137	SSTc2d J032741.5+302017	-1.02 ± 0.03	1.22	1.32 ± 0.15	2.21	3.21 ± 0.29
10	J032747.68+301204.4	51.9486767	30.2012397	NAME LDN 1455 IRS 2	-0.11 ± 0.04	2.68	3.26 ± 0.22	2.88	6.92 ± 0.39
11	J032800.09+300846.9	52.0004148	30.1463655	2MASS J03280010+3008469	-1.4 ± 0.04	1.34	1.38 ± 0.27	3.47	3.47 ± 0.39
12	J032842.43+302953.1	52.1768142	30.4980955	[EJ2009] 146	-0.91 ± 0.04	0.39	0.63 ± 0.14	1.91	1.9 ± 0.33
13	J032843.26+311732.9	52.1802544	31.2924824	HBC 340	-0.12 ± 0.04	1.48	2.12 ± 0.12	1.89	0.51 ± 0.42
14	J032843.55+311736.6	52.1814862	31.2935018	HBC 341	-0.29 ± 0.06	3.17	1.47 ± 0.11	0.87	2.09 ± 0.42
15	J032846.19+311638.6	52.192479	31.2773971	EM* LkHA 351	-1.57 ± 0.04	1.33	1.37 ± 0.45	2.51	2.3 ± 0.25
16	J032847.83+311655.2	52.1992954	31.2820006	2MASS J03284782+3116552	-0.96 ± 0.04	1.29	0.58 ± 0.47	3.3	1.39 ± 0.53
17	J032851.02+311818.4	52.212614	31.3051357	EM* LkHA 352A	-0.74 ± 0.04	2.61	2.19 ± 0.13	8.35	6.61 ± 0.36
18	J032851.19+311954.8	52.2133275	31.3319087	2MASS J03285119+3119548	-0.42 ± 0.04	2.78	1.52 ± 0.07	0.92	1.35 ± 0.3
19	J032852.16+312245.3	52.2173627	31.3792507	2MASS J03285216+3122453	-1.0 ± 0.04	1.47	1.4 ± 0.07	9.36	7.52 ± 0.21
20	J032852.18+304505.5	52.217418	30.7515404	2MASS J03285217+3045055	-0.78 ± 0.04	1.99	2.14 ± 0.17	9.84	7.13 ± 0.09
21	J032854.62+311651.3	52.2275887	31.2809407	2MASS J03285461+3116512	-0.99 ± 0.04	1.95	1.79 ± 0.43	7.29	8.18 ± 0.37
22	J032856.64+311835.6	52.2360079	31.30989	2MASS J03285663+3118356	-0.85 ± 0.04	2.64	1.83 ± 0.19	6.25	5.75 ± 0.24
23	J032856.96+311622.3	52.2481447	31.27287	2MASS J03285694+3116222	-0.49 ± 0.04	1.58	1.6 ± 0.06	8.48	7.48 ± 0.45
24	J032859.55+312146.7	52.2481447	31.3629832	EM* LkHA 353	-1.22 ± 0.04	2.28	2.32 ± 1.12	7.65	6.67 ± 0.11
25	J032903.77+311603.8	52.2657417	31.2677457	V* V512 Per	0.77 ± 0.04	1.22	25.69 ± 0.09	1.73	3.73 ± 1.09
26	J032903.86+312148.7	52.2661055	31.3635495	2MASS J03290386+3121487	-1.23 ± 0.04	1.98	2.37 ± 0.16	8.22	7.29 ± 0.09
27	J032917.67+312244.9	52.3236529	31.3791443	NAME NGC 1333 IRS 2	-1.1 ± 0.04	2.17	2.49 ± 0.16	4.94	0.54 ± 0.56
28	J032918.72+312325.5	52.3280363	31.3904245	2MASS J03291872+3123254	0.09 ± 0.04	1.82	1.34 ± 0.11	4.75	1.94 ± 0.33
29	J032919.77+312457.1	52.3324158	31.4158781	2MASS J03291977+3124572	0.14 ± 0.04	2.56	2.55 ± 0.1	3.95	3.78 ± 0.23
30	J032921.55+312110.3	52.3398199	31.3528862	2MASS J03292155+3121104	-0.88 ± 0.05	1.17	0.95 ± 0.13	6.03	6.88 ± 0.16
31	J032921.87+311536.2	52.3411571	31.2600729	EM* LkHA 271	-1.53 ± 0.04	1.08	1.82 ± 0.09	7.46	2.46 ± 0.28
32	J032923.15+312030.3	52.3464585	31.3447503	EM* LkHA 355	-0.89 ± 0.04	1.48	0.96 ± 0.32	8.59	4.59 ± 0.19
33	J032923.23+312653.0	52.3468186	31.4480694	2MASS J03292322+3126531	-0.53 ± 0.04	0.39	0.39 ± 0.1	5.14	3.8 ± 0.38
34	J032925.92+312640.1	52.3580264	31.4444756	2MASS J03292591+3126401	-0.78 ± 0.03	1.48	1.87 ± 0.09	2.24	2.38 ± 0.4
35	J032926.79+312647.4	52.3616596	31.44652	2MASS J03292681+3126475	-1.94 ± 0.05	1.6	1.39 ± 0.16	5.2	3.44 ± 0.25

Table 3—Continued

Order	Catalog Number	RA (deg)	Dec (deg)	Name	$\alpha$	Mass <sub>BF</sub> (M <sub>⊙</sub> )	Mass <sub>peak</sub> (M <sub>⊙</sub> )	Age <sub>BF</sub> (Myr)	Age <sub>peak</sub> (Myr)
36	J032928.89+305841.8	52.3703977	30.978281	[EDJ2009] 248	-0.77 ± 0.04	0.23	0.33 ± 0.29	5.25	4.26 ± 0.21
37	J032929.26+311834.7	52.371941	31.309651	2MASS J03292925+3118347	-1.34 ± 0.04	0.36	0.51 ± 0.19	2.17	2.42 ± 0.41
38	J032929.78+312102.6	52.3741039	31.3507368	2MASS J03292978+3121027	-0.69 ± 0.04	0.43	0.73 ± 0.12	2.68	2.67 ± 0.26
39	J032930.39+311903.3	52.3766345	31.3176101	EM* LkHA 356	-1.13 ± 0.04	2.01	1.82 ± 0.15	8.07	7.42 ± 0.65
40	J032932.56+312436.9	52.38569	31.4102637	EM* LkHA 357	-0.92 ± 0.04	0.55	0.43 ± 0.11	6.42	6.05 ± 0.22
41	J032932.87+312712.5	52.3869611	31.4534793	2MASS J03293286+3127126	-1.11 ± 0.06	0.22	0.41 ± 0.23	4.8	9.09 ± 0.18
42	J032954.03+312053.0	52.475129	31.3480571	2MASS J03295403+3120529	-0.64 ± 0.04	0.43	0.56 ± 0.17	2.68	2.88 ± 0.34
43	J033024.09+311404.3	52.6004078	31.2345343	2MASS J03302409+3114043	-0.98 ± 0.05	0.22	0.27 ± 0.07	6.61	8.04 ± 0.13
44	J033035.94+303024.5	52.6497626	30.5068066	2MASS J03303593+3030244	-0.96 ± 0.04	3.29	2.99 ± 0.12	1.09	1.17 ± 0.36
45	J033036.97+303127.7	52.6540781	30.5243642	SSTc2d J033037.0+303128	-1.16 ± 0.04	2.87	2.38 ± 0.1	7.94	1.09 ± 0.52
46	J033043.99+303246.9	52.683332	30.5463736	[EDJ2009] 269	-0.99 ± 0.04	2.44	2.22 ± 0.16	6.73	0.78 ± 0.45
47	J033052.52+305417.7	52.7188596	30.9049298	2MASS J03305252+3054177	-0.47 ± 0.04	0.12	0.12 ± 0.25	0.1	0.18 ± 0.29
48	J033110.70+304940.5	52.7945859	30.8279314	SSTc2d J033110.7+304941	-0.61 ± 0.04	0.57	0.32 ± 0.25	2.11	1.15 ± 0.36
49	J033114.71+304955.3	52.811322	30.8320395	[EDJ2009] 272	-0.45 ± 0.04	0.11	0.13 ± 0.12	0.62	0.09 ± 0.56
50	J033118.31+304939.4	52.8263068	30.8276353	SSTc2d J033118.3+304940	-0.71 ± 0.04	1.48	2.13 ± 0.14	2.24	0.78 ± 0.3
51	J033120.11+304917.5	52.8338214	30.8215501	[EDJ2009] 274	-0.75 ± 0.04	0.37	0.36 ± 0.17	0.04	0.04 ± 0.37
52	J033128.87+303053.2	52.8703166	30.5147946	2MASS J03312887+3030531	-1.57 ± 0.04	2.25	1.69 ± 0.35	2.13	0.87 ± 0.25
53	J033142.41+310624.7	52.9267459	31.106877	[EDJ2009] 278	-1.45 ± 0.04	0.48	0.64 ± 0.13	2.14	1.83 ± 0.46
54	J033233.00+310221.6	53.1375316	31.0393575	[EDJ2009] 281	-1.02 ± 0.04	1.29	1.4 ± 0.12	3.3	1.26 ± 0.27
55	J033234.06+310055.7	53.1419191	31.0154864	IRAS 03295+3050	-0.94 ± 0.04	2.17	1.64 ± 0.52	1.69	0.95 ± 0.33
56	J033241.70+311045.7	53.1737635	31.1793821	2MASS J03324171+3110461	-0.45 ± 0.03	0.27	1.44 ± 0.09	1.58	0.94 ± 0.48
57	J033312.84+312124.1	53.3035245	31.3566981	SSTc2d J033312.8+312124	0.01 ± 0.04	2.37	3.14 ± 0.05	7.2	3.01 ± 0.37
58	J033330.42+311050.4	53.3767691	31.180692	EM* LkHA 327	-1.24 ± 0.05	2.69	2.98 ± 0.32	3.24	7.86 ± 0.21
59	J033341.30+311340.9	53.4220887	31.2280551	2MASS J03334129+3113410	-0.85 ± 0.04	1.08	0.45 ± 0.23	7.46	0.68 ± 1.0
60	J033346.93+305350.1	53.4455792	30.8972686	[EDJ2009] 299	-1.1 ± 0.06	0.16	0.28 ± 0.24	8.87	4.15 ± 0.18
61	J033401.67+311439.6	53.5069625	31.2443577	EM* LkHA 328	-0.97 ± 0.04	1.47	1.57 ± 0.18	1.19	0.95 ± 0.24
62	J033430.79+311324.3	53.6283159	31.2234194	[EDJ2009] 302	-1.03 ± 0.05	0.18	0.57 ± 0.16	3.06	5.64 ± 0.21
63	J033449.86+311550.1	53.7077643	31.263929	2MASS J03344987+3115498	-1.42 ± 0.04	0.73	1.47 ± 0.12	0.97	1.81 ± 0.21
64	J033711.38+330303.0	54.2974288	33.0508484	2MASS J03371138+3303032	-0.95 ± 0.03	1.25	1.69 ± 0.19	1.97	2.56 ± 0.32
65	J034109.14+314437.9	55.2880837	31.7438668	IRAS 03380+3135	-1.5 ± 0.04	0.63	2.59 ± 0.12	0.47	0.52 ± 0.31
66	J034114.12+315946.1	55.308873	31.996148	2MASS J03411412+3159462	-1.88 ± 0.05	1.97	2.04 ± 0.14	9.79	8.31 ± 0.1
67	J034157.45+314836.6	55.4894069	31.810175	[EDJ2009] 314	-1.27 ± 0.04	2.28	2.21 ± 0.36	7.82	8.39 ± 0.62
68	J034157.76+314800.7	55.490705	31.8002143	[EDJ2009] 315	-0.89 ± 0.04	0.42	1.73 ± 0.1	0.45	0.87 ± 0.37
69	J034204.35+314711.4	55.5181477	31.7865217	[EDJ2009] 319	-0.84 ± 0.04	0.43	0.21 ± 0.39	1.81	1.83 ± 0.44
70	J034219.28+314326.8	55.5803535	31.7241352	2MASS J03421927+3143269	-0.8 ± 0.04	1.08	1.17 ± 0.26	7.46	0.98 ± 0.34

Table 3—Continued

Order	Catalog Number	RA (deg)	Dec (deg)	Name	$\alpha$	Mass <sub>BF</sub> (M <sub>⊙</sub> )	Mass <sub>peak</sub> (M <sub>⊙</sub> )	Age <sub>BF</sub> (Myr)	Age <sub>peak</sub> (Myr)
71	J034220.34+320530.9	55.584758	32.0919442	2MASS J03422033+3205310	-0.94 ± 0.05	0.42	0.37 ± 0.04	7.36	2.79 ± 0.31
72	J034223.33+315742.6	55.5972411	31.9618447	[C93] 46	-1.73 ± 0.04	1.97	1.87 ± 0.18	9.79	8.62 ± 0.08
73	J034232.92+314220.5	55.6371724	31.7057131	[EDJ2009] 326	-0.58 ± 0.04	0.45	0.57 ± 0.06	3.15	1.83 ± 0.51
74	J034254.70+314345.1	55.7279365	31.7292217	[EDJ2009] 332	-1.4 ± 0.05	1.41	1.43 ± 0.19	3.38	5.77 ± 0.19
75	J034255.96+315841.9	55.7331887	31.9783205	2MASS J03425596+3158419	-0.36 ± 0.03	2.14	1.97 ± 0.08	0.65	0.6 ± 0.17
76	J034306.80+314820.4	55.7783399	31.8056847	[EDJ2009] 336	-1.89 ± 0.08	0.26	0.8 ± 0.07	1.57	3.02 ± 0.28
77	J034328.20+320159.1	55.8675276	32.0331078	V* V338 Per	-1.4 ± 0.05	0.75	1.33 ± 0.08	2.11	2.13 ± 0.27
78	J034344.49+314309.3	55.9353919	31.7192681	2MASS J03434449+3143092	-0.83 ± 0.04	0.8	0.83 ± 0.14	1.05	1.18 ± 0.67
79	J034344.61+320817.7	55.9359083	32.1382646	2MASS J03434461+3208177	-0.94 ± 0.05	0.76	0.71 ± 0.08	2.77	2.34 ± 0.28
80	J034345.16+320358.6	55.9381899	32.0663019	2MASS J03434517+3203585	0.37 ± 0.03	2.44	2.05 ± 0.25	6.73	6.45 ± 0.64
81	J034348.81+321551.4	55.9534082	32.2643026	2MASS J03434881+3215515	-0.8 ± 0.05	0.39	0.39 ± 0.32	5.14	4.91 ± 0.32
82	J034356.03+320213.2	55.9834625	32.0370212	2MASS J03435602+3202132	-1.07 ± 0.04	0.69	1.62 ± 0.14	0.37	0.67 ± 0.47
83	J034358.12+321357.0	55.9922053	32.2325024	C1* IC 348 LRL 323	0.21 ± 0.07	0.3	0.23 ± 0.16	8.02	8.86 ± 0.3
84	J034358.56+321727.5	55.9940193	32.2909808	2MASS J03435856+3217275	-0.93 ± 0.04	1.84	1.0 ± 0.29	3.06	3.21 ± 0.27
85	J034358.90+321127.1	55.9954458	32.1908736	2MASS J03435890+3211270	-1.06 ± 0.06	0.18	0.59 ± 0.38	0.18	0.95 ± 0.5
86	J034359.09+321421.3	55.9962085	32.2392547	2MASS J03435907+3214213	-0.26 ± 0.05	0.55	0.79 ± 0.05	6.41	6.45 ± 0.67
87	J034359.64+320154.0	55.9985229	32.0316944	2MASS J03435964+3201539	-0.53 ± 0.04	3.03	2.46 ± 0.31	2.7	8.51 ± 0.2
88	J034406.78+320754.0	56.028277	32.1316908	2MASS J03440678+3207540	-0.35 ± 0.05	0.14	0.45 ± 0.07	1.03	6.33 ± 0.41
89	J034408.47+320716.5	56.0353011	32.1212639	HD 281160	-1.71 ± 0.04	1.97	1.92 ± 0.08	9.79	7.81 ± 0.44
90	J034409.14+320709.3	56.0381115	32.1192589	BD+31 641A	-1.5 ± 0.04	1.97	1.95 ± 0.41	9.79	9.48 ± 0.1
91	J034411.62+320313.1	56.048419	32.0536554	2MASS J03441162+3203131	-0.94 ± 0.04	1.19	1.48 ± 0.24	1.33	0.98 ± 0.46
92	J034418.16+320456.9	56.0756684	32.0824977	2MASS J03441816+3204570	-1.13 ± 0.09	0.29	0.45 ± 0.33	0.17	0.48 ± 0.39
93	J034421.61+321037.7	56.0900646	32.1771427		-0.63 ± 0.04	1.08	0.97 ± 0.26	7.46	1.01 ± 0.45
94	J034422.29+320542.6	56.0928827	32.0951789		0.35 ± 0.05	1.63	1.46 ± 0.08	4.83	3.3 ± 0.58
95	J034422.34+321200.4	56.0930856	32.200113		-1.22 ± 0.04	1.87	1.41 ± 0.14	6.19	9.21 ± 0.16
96	J034422.57+320153.6	56.0940739	32.0315756	2MASS J03442257+3201536	-0.79 ± 0.04	2.55	2.43 ± 0.37	5.91	5.96 ± 0.44
97	J034426.68+320820.5	56.1111899	32.1390304	2MASS J03442668+3208203	-0.5 ± 0.05	1.34	1.61 ± 0.3	5.24	2.25 ± 0.47
98	J034427.21+322028.7	56.1133914	32.3413181	2MASS J03442721+3220288	-0.45 ± 0.07	0.25	0.28 ± 0.16	4.28	4.03 ± 0.22
99	J034427.24+321420.9	56.1135363	32.2391618		-1.09 ± 0.1	0.6	0.54 ± 0.1	6.02	4.57 ± 0.23
100	J034427.89+322718.9	56.1162134	32.4552638	2MASS J03442789+3227189	-1.09 ± 0.04	0.17	0.16 ± 0.11	1.23	0.51 ± 0.34
101	J034428.50+315954.0	56.1187879	31.9983367		-1.42 ± 0.05	0.88	0.93 ± 0.1	8.15	4.95 ± 0.2
102	J034429.73+321039.6	56.1238824	32.1776775		-0.28 ± 0.04	1.58	1.41 ± 0.14	0.94	3.32 ± 0.27
103	J034429.79+320054.6	56.1241648	32.0151765		-0.72 ± 0.06	0.66	0.77 ± 0.12	8.28	6.47 ± 0.38
104	J034430.82+320955.8	56.1284416	32.1655078	2MASS J03443081+3209558	-0.17 ± 0.05	2.65	2.33 ± 0.06	6.09	6.74 ± 0.17
105	J034431.20+320622.1	56.1300119	32.1061402	V* V705 Per	-2.49 ± 0.11	2.09	2.56 ± 0.23	5.35	2.6 ± 0.25

Table 3—Continued

Order	Catalog Number	RA (deg)	Dec (deg)	Name	$\alpha$	Mass <sub>BF</sub> (M <sub>⊙</sub> )	Mass <sub>peak</sub> (M <sub>⊙</sub> )	Age <sub>BF</sub> (Myr)	Age <sub>peak</sub> (Myr)
106	J034432.03+321143.7	56.1334627	32.1954928	Cl* IC 348 H 140	0.28 ± 0.04	2.23	2.22 ± 0.13	6.52	0.46 ± 0.61
107	J034434.20+320946.4	56.1425188	32.1629105	BD+31 643A	-2.07 ± 0.05	3.13	3.31 ± 0.16	2.07	2.42 ± 0.62
108	J034434.80+315655.2	56.1450193	31.9486743	2MASS J03443481+3156552	-1.4 ± 0.05	0.98	0.63 ± 0.28	4.09	7.89 ± 0.32
109	J034434.97+321531.1	56.145737	32.2586537	2MASS J03443498+3215311	-0.3 ± 0.06	0.57	0.57 ± 0.07	2.83	4.64 ± 0.22
110	J034435.35+321004.5	56.1473265	32.1679432	2MASS J03443536+3210045	-1.19 ± 0.04	2.55	3.22 ± 0.24	3.65	2.39 ± 0.29
111	J034435.67+320303.6	56.1486569	32.0510013	2MASS J03443568+3203035	0.13 ± 0.04	0.47	0.95 ± 0.1	9.51	7.89 ± 0.46
112	J034436.94+320645.3	56.1539579	32.1125835	V* V918 Per	-1.92 ± 0.08	1.97	2.1 ± 0.11	1.55	0.79 ± 0.17
113	J034437.40+320901.0	56.1558428	32.1502995	V* V710 Per	0.16 ± 0.06	2.22	1.51 ± 0.16	2.9	3.65 ± 0.25
114	J034437.88+320804.0	56.1578576	32.1344452	V* V920 Per	-1.66 ± 0.13	1.73	1.55 ± 0.14	7.67	1.01 ± 0.3
115	J034437.96+320329.7	56.1582056	32.0582586	V* V712 Per	-0.16 ± 0.04	1.26	1.65 ± 0.11	2.38	3.48 ± 0.33
116	J034438.00+321137.0	56.1583528	32.193614	V* V713 Per	-1.16 ± 0.17	0.77	0.16 ± 0.99	5.56	5.98 ± 0.42
117	J034438.17+321021.2	56.1590704	32.1725691	2MASS J03443814+3210215	0.54 ± 0.19	5.13	25.69 ± 0.28	0.04	0.52 ± 0.86
118	J034438.44+320735.7	56.1601957	32.1266101	V* V715 Per	-0.64 ± 0.08	1.64	1.53 ± 0.77	4.5	0.98 ± 0.34
119	J034438.72+320843.0	56.1613728	32.1452907	V* V717 Per	-1.29 ± 0.33	0.57	1.79 ± 0.14	0.01	3.72 ± 1.09
120	J034439.16+320918.4	56.1631908	32.1551189	V* V921 Per	-1.38 ± 0.07	2.68	1.41 ± 0.32	1.18	1.28 ± 0.21
121	J034439.78+321804.0	56.1657808	32.3011331	2MASS J03443979+3218041	-0.82 ± 0.06	0.82	0.81 ± 0.34	4.22	1.71 ± 0.35
122	J034441.73+321202.3	56.1738994	32.2006505	2MASS J03444173+3212022	0.14 ± 0.04	0.49	0.22 ± 0.2	1.37	1.46 ± 0.78
123	J034442.09+320901.2	56.1753791	32.1503355	Cl* IC 348 CB 119	-0.72 ± 0.05	0.55	0.54 ± 0.2	0.67	1.09 ± 0.55
124	J034442.56+321002.4	56.1773661	32.1673597	2MASS J03444256+3210025	0.02 ± 0.07	0.18	0.14 ± 0.51	0.27	0.44 ± 0.49
125	J034443.76+321030.3	56.1823352	32.1751	V* V719 Per	-0.25 ± 0.05	1.14	1.35 ± 0.33	9.65	3.75 ± 0.58
126	J034444.59+320812.5	56.1857922	32.136829	V* V925 Per	-0.21 ± 0.07	0.57	1.35 ± 0.15	3.76	4.23 ± 0.38
127	J034444.70+320402.5	56.18629	32.0673732	V* V926 Per	-1.04 ± 0.04	1.85	1.61 ± 0.08	6.92	0.8 ± 0.39
128	J034447.71+321911.8	56.1988298	32.3199551	[C93] 80	-0.98 ± 0.05	1.78	1.58 ± 0.06	7.63	2.96 ± 0.24
129	J034450.65+321906.4	56.2110465	32.3184715	V* V927 Per	-2.4 ± 0.09	2.24	2.58 ± 0.37	4.19	2.73 ± 0.18
130	J034456.13+320915.0	56.2338955	32.1541925	2MASS J03445614+3209152	-1.44 ± 0.1	1.98	1.64 ± 0.05	3.3	2.35 ± 0.43
131	J034501.41+320501.7	56.2558937	32.0838185	2MASS J03450142+3205017	-2.04 ± 0.05	1.56	1.81 ± 0.07	8.36	4.09 ± 0.26
132	J034501.51+321051.3	56.2566323	32.1809357	2MASS J03450151+3210512	-0.73 ± 0.06	0.94	0.93 ± 0.14	3.65	8.05 ± 0.13
133	J034501.74+321427.6	56.2572626	32.2410271	2MASS J03450174+3214276	-1.24 ± 0.04	1.41	1.17 ± 0.08	3.38	2.84 ± 0.25
134	J034507.62+321027.9	56.2817792	32.1744282	2MASS J03450762+3210279	-1.75 ± 0.05	1.64	1.56 ± 0.05	7.44	2.82 ± 0.33
135	J034514.71+294503.1	56.3113186	29.7508854	HD 281192	-1.09 ± 0.06	2.87	2.85 ± 0.26	4.67	4.32 ± 0.23
136	J034516.34+320619.9	56.3180861	32.1055416	EM* LkHA 99	-0.8 ± 0.04	2.29	1.5 ± 0.15	7.17	0.59 ± 0.17
137	J034520.45+320634.4	56.3352286	32.1095804	2MASS J03452046+3206344	-1.15 ± 0.04	2.16	2.05 ± 0.24	2.02	2.44 ± 0.39
138	J034525.14+320930.3	56.3547711	32.1584269	2MASS J03452514+3209301	-0.79 ± 0.04	0.57	0.53 ± 0.27	3.11	1.11 ± 0.3
139	J034536.85+322556.8	56.4035733	32.4324705	EM* LkHA 329	-1.31 ± 0.04	1.25	1.43 ± 0.14	0.65	0.67 ± 0.28
140	J034548.28+322411.8	56.4512063	32.4032995	IRAS 03426+3214	-1.82 ± 0.06	2.46	3.11 ± 0.1	3.92	0.5 ± 0.31



Table 3—Continued

Order	Catalog Number	RA (deg)	Dec (deg)	Name	$\alpha$	Mass <sub>BF</sub> (M <sub>⊙</sub> )	Mass <sub>peak</sub> (M <sub>⊙</sub> )	Age <sub>BF</sub> (Myr)	Age <sub>peak</sub> (Myr)
141	J034747.14+330403.2	56.9464261	33.0675598	[OH83] B5 3	-0.55 ± 0.03	0.56	1.81 ± 0.16	1.41	1.41 ± 0.23
142	J034929.05+345800.6	57.3710713	34.9668454	2MASS J03492906+3458006	-0.89 ± 0.04	2.36	3.13 ± 0.16	3.15	0.07 ± 0.93
143	J040443.06+261856.3	61.1794518	26.3156406	IRAS 04016+2610	0.29 ± 0.04	0.77	0.63 ± 0.1	0.01	0.01 ± 0.52
144	J041320.01+311047.2	63.3334141	31.1797938	HD 281789	0.23 ± 0.04	4.31	4.24 ± 0.43	0.7	1.96 ± 0.75
145	J041353.28+281123.1	63.4720167	28.1897541	IRAS 04108+2803A	-0.08 ± 0.04	0.49	1.65 ± 0.08	0.25	0.59 ± 0.48
146	J041357.38+291819.1	63.4890872	29.305319	IRAS 04108+2910	-0.78 ± 0.03	0.6	0.62 ± 0.06	0.42	0.16 ± 0.31
147	J041413.58+281249.0	63.5566088	28.2136261	V* FM Tau	-0.78 ± 0.03	1.86	2.3 ± 0.39	8.41	8.21 ± 0.58
148	J041414.59+282757.9	63.5608221	28.4661111	V* FN Tau	-0.37 ± 0.04	3.97	2.79 ± 0.07	3.9	0.41 ± 0.65
149	J041417.00+281057.6	63.5708561	28.1826907	V* CW Tau	-1.48 ± 0.07	3.74	2.91 ± 0.12	9.87	4.01 ± 0.18
150	J041417.61+280609.5	63.5733926	28.1026472	[BCG93] 1	-0.3 ± 0.03	0.29	1.64 ± 0.1	0.22	0.64 ± 0.72
151	J041426.27+280603.1	63.6094781	28.1008827	[BHS98] MHO 1	-0.68 ± 0.08	4.02	3.63 ± 0.1	1.13	7.83 ± 0.76
152	J041430.55+280514.4	63.6272982	28.0873454	NAME IRAS 04114+2757G	0.2 ± 0.04	3.5	3.54 ± 0.07	8.06	3.92 ± 0.23
153	J041447.30+264626.3	63.697116	26.7739795	V* FP Tau	-1.47 ± 0.03	0.4	0.42 ± 0.22	0.29	0.52 ± 0.21
154	J041447.86+264810.9	63.6994418	26.8030313	V* CX Tau	-0.72 ± 0.03	0.44	0.42 ± 0.3	0.14	0.27 ± 0.32
155	J041449.28+281230.3	63.705357	28.2084404	V* FO Tau	-1.19 ± 0.04	3.02	2.04 ± 0.23	0.48	0.65 ± 0.3
156	J041539.16+281858.3	63.9132044	28.3162091	2MASS J04153916+2818586	-1.49 ± 0.04	0.44	1.79 ± 0.15	0.4	0.67 ± 0.31

Table 4. Physical parameters measured for the 66 AGB candidates

Order	Catalog Number	RA (deg)	Dec (deg)	Name	$\alpha$	Mass <sub>BF</sub> ( $M_{\odot}$ )	Mass <sub>peak</sub> ( $M_{\odot}$ )	Age <sub>BF</sub> (Myr)	Age <sub>peak</sub> (Myr)
1	J03231.00+311527.2	50.629184	31.25754		-2.62 ± 0.04	2.54	2.8	1.04	1.12
2	J032241.26+341237.4	50.671772	34.210327	V* LY Per	-2.67 ± 0.11	3.7	3.71	0.3	0.34
3	J032243.15+364540.1	50.679838	36.761158		-2.6 ± 0.05	0.41	0.52	0.49	0.51
4	J032244.12+355315.0	50.68377	35.887527		-2.65 ± 0.04	0.41	0.5	0.49	0.48
5	J032421.19+334023.3	51.0883	33.673141		-2.36 ± 0.05	0.81	0.78	0.17	0.16
6	J032429.84+341710.0	51.124323	34.286106	HD 20994	-2.66 ± 0.04	1.93	1.91	7.05	7.33
7	J032435.96+351836.8	51.149879	35.3102	TYC 2349-915-1	-2.05 ± 0.11	4.24	4.29	0.49	0.44
8	J032442.56+311554.9	51.177375	31.265232		-2.28 ± 0.04	0.82	0.53	0.55	0.44
9	J032740.52+311539.2	51.91891	31.2609	BD+30 543	-2.57 ± 0.04	2.21	1.94	4.57	5.79
10	J032810.45+332844.3	52.043516	33.478863	NSV 1151	-2.37 ± 0.48	17.26	25.69	0.09	3.72
11	J033110.80+284231.2	52.794686	28.708618	TYC 1810-104-1	-1.91 ± 0.02	5.57	5.63	0.14	0.12
12	J033238.02+295708.7	53.158482	29.952421	IRAS 03295+2947	-2.54 ± 0.07	3.46	2.84	1.27	0.6
13	J033251.29+332210.9	53.213706	33.369652	NIPSS 277C21	-2.24 ± 0.05	0.55	0.51	0.34	0.49
14	J033446.72+345157.9	53.694653	34.866066	2MASS J03344671+3451578	-2.57 ± 0.06	0.81	0.78	0.17	0.19
15	J033603.04+313900.6	54.012667	31.650137		-2.07 ± 0.04	0.41	0.37	0.49	0.55
16	J033606.72+292405.6	54.028058	29.40156	IRAS 03330+2914	-2.01 ± 0.09	1.28	1.26	0.15	0.14
17	J033628.62+315539.3	54.119444	31.927509	[KSP2003] J033628.70+315540.1	-2.63 ± 0.05	1.64	1.64	0.09	0.18
18	J033652.31+305348.5	54.218042	30.896807	IRAS 03337+3043	-2.1 ± 0.06	3.8	3.33	0.83	1.35
19	J033819.09+320313.5	54.579494	32.053757	V* V734 Per	-2.42 ± 0.1	3.7	3.69	0.3	0.31
20	J033829.54+344014.6	54.62315	34.670719	V* V735 Per	-2.37 ± 0.06	3.39	3.07	1.37	1.07
21	J033956.08+305601.1	54.983683	30.933563		-2.58 ± 0.04	2.53	1.78	2.69	1.87
22	J034025.22+303304.5	55.10511	30.551268		-2.37 ± 0.05	2.42	2.57	1.15	1.2
23	J034057.79+311805.9	55.240823	31.301645	V* V900 Per	-2.59 ± 0.05	1.93	1.92	7.05	6.84
24	J034222.38+363037.0	55.593101	36.510273	V* AF Per	-2.54 ± 0.53	5.57	5.57	0.14	0.14
25	J034311.08+321746.4	55.796156	32.296204		-2.59 ± 0.05	3.41	2.65	1.19	2.03
26	J034402.53+360732.5	56.010547	36.125698		-2.6 ± 0.04	0.36	0.36	0.6	0.59
27	J034404.68+293216.5	56.019508	29.537918	HD 281161	-2.63 ± 0.04	1.67	1.84	1.18	1.39
28	J034429.97+322558.8	56.124909	32.433029	HD 23478	-2.55 ± 0.05	1.93	1.52	7.05	9.39
29	J034430.35+322152.8	56.126505	32.364689		-2.38 ± 0.05	0.8	0.95	3.02	1.96
30	J034547.88+320058.6	56.449552	32.016258		-2.41 ± 0.04	1.93	1.94	7.05	7.34
31	J034640.87+321724.6	56.670314	32.290203	IRAS 03437+3720	-2.48 ± 0.05	3.06	3.05	2.5	2.5
32	J034701.91+372921.3	56.757843	37.489201	V* V1190 Tau	-2.51 ± 0.11	2.84	2.83	0.23	0.35
33	J034733.76+295851.3	56.89075	29.98098	IRAS 03446+3709	-2.57 ± 0.06	0.64	0.74	0.38	0.47
34	J034750.97+371843.4	56.962434	37.312069		-2.49 ± 0.05	0.71	0.72	0.5	0.48
35	J034935.66+263033.8	57.3987	26.509445	V* BI Tau	-2.6 ± 0.06	3.17	3.04	1.15	1.28

Table 4—Continued

Order	Catalog Number	RA (deg)	Dec (deg)	Name	$\alpha$	Mass <sub>BF</sub> (M <sub>⊙</sub> )	Mass <sub>peak</sub> (M <sub>⊙</sub> )	Age <sub>BF</sub> (Myr)	Age <sub>peak</sub> (Myr)
36	J034936.08+363441.3	57.400339	36.578152		-2.64 ± 0.04	0.35	0.36	0.76	0.75
37	J035028.16+274005.4	57.617117	27.668297	V* V1192 Tau	-2.42 ± 0.13	3.41	3.42	0.08	0.07
38	J035103.41+362849.8	57.764296	36.480648	IRAS 03478+3619	-2.65 ± 0.12	1.64	1.82	0.09	0.1
39	J035124.25+361528.7	57.851054	36.257935	V* V377 Per	-2.27 ± 0.04	0.34	0.37	0.5	0.57
40	J035132.31+372509.4	57.88466	37.4193	IRAS 03482+3716	-2.53 ± 0.06	0.64	0.76	0.38	0.42
41	J035245.26+372608.4	58.188624	37.43565		-2.65 ± 0.05	0.41	0.4	0.49	0.47
42	J035402.26+363218.3	58.509482	36.538235	V* V637 Per	-1.16 ± 0.02	6.71	6.92	0.04	0.03
43	J035448.08+344520.7	58.700441	34.755768		-2.62 ± 0.04	0.41	0.43	0.49	0.5
44	J035801.79+365502.2	59.507468	36.917244		-2.63 ± 0.04	0.36	0.34	0.6	0.79
45	J035936.33+313651.4	59.901339	31.61425	IRAS 03564+3128	-2.21 ± 0.05	0.52	0.5	0.26	0.39
46	J035946.41+344056.4	59.943341	34.682392	V* V739 Per	-2.59 ± 0.09	3.7	2.85	0.3	0.3
47	J040207.33+302353.6	60.530554	30.398191		-2.31 ± 0.04	1.26	0.77	0.73	0.77
48	J040229.82+360656.5	60.624242	36.115685	IRAS 03592+3558	-2.49 ± 0.07	1.07	1.51	0.27	0.23
49	J040233.34+282951.5	60.638931	28.497602	GSC 01825-00286	-2.37 ± 0.09	1.17	1.64	0.14	0.14
50	J040536.53+320230.1	61.40227	32.041737	IRAS 04024+3154	-2.24 ± 0.06	0.84	0.57	0.28	0.43
51	J040610.35+303928.8	61.543103	30.657948		-2.65 ± 0.05	0.82	0.85	0.43	0.45
52	J040733.34+350211.1	61.888932	35.036388		-2.48 ± 0.04	0.41	0.42	0.49	0.58
53	J040828.00+363219.6	62.116687	36.538727	IRAS 04051+3624	-2.25 ± 0.09	5.87	3.94	4.18	2.45
54	J040833.90+265034.7	62.141092	26.843029	V* TV Tau	-2.45 ± 0.11	7.21	7.02	1.38	1.39
55	J040847.99+313053.8	62.199979	31.514896	V* V743 Per	-2.64 ± 0.05	0.55	0.56	0.41	0.41
56	J040853.64+371045.6	62.223552	37.179352		-2.46 ± 0.04	0.35	0.38	0.79	0.72
57	J040936.96+332937.1	62.404023	33.493721	V* V394 Per	-1.98 ± 0.03	2.8	2.7	0.14	0.14
58	J040953.65+321154.0	62.473612	32.198292	IRAS 04067+3204	-2.29 ± 0.06	0.81	0.72	0.17	0.23
59	J040954.92+353419.2	62.478869	35.572006		-2.63 ± 0.05	0.53	0.54	0.47	0.47
60	J041047.04+371351.4	62.69601	37.230907		-2.58 ± 0.05	0.47	0.5	0.43	0.44
61	J041142.35+262718.2	62.926491	26.455038	V* V1247 Tau	-2.51 ± 0.07	1.07	1.74	0.27	0.48
62	J041315.68+332955.4	63.315343	33.498722	2MASS J04131568+3329553	-1.89 ± 0.11	1.64	2.91	0.09	0.15
63	J041343.47+262456.6	63.431257	26.415569	V* V482 Tau	-1.33 ± 0.16	7.26	4.32	0.04	0.02
64	J041422.36+342522.6	63.593223	34.422928		-2.43 ± 0.04	0.41	0.39	0.49	0.48
65	J041424.50+363642.9	63.602068	36.611908		-2.44 ± 0.04	0.4	0.36	0.92	1.29
66	J041516.84+355414.6	63.820108	35.904034	2MASS J04151682+3554145	-2.64 ± 0.08	0.81	0.82	0.17	0.15

- Rebull, L. M., Stapelfeldt, K. R., Evans, II, N. J., et al. 2007, *ApJS*, 171, 447
- Rebull, L. M., Padgett, D. L., McCabe, C.-E., et al. 2010, *ApJS*, 186, 259
- Rebull, L. M., Koenig, X. P., Padgett, D. L., et al. 2011, *ApJS*, 196, 4
- Ridge, N. A., Di Francesco, J., Kirk, H., et al. 2006, *AJ*, 131, 2921
- Robitaille, T. P., Whitney, B. A., Indebetouw, R., & Wood, K. 2007, *ApJS*, 169, 328
- Robitaille, T. P., Whitney, B. A., Indebetouw, R., Wood, K., & Denzmore, P. 2006, *ApJS*, 167, 256
- Roeser, S., Demleitner, M., & Schilbach, E. 2010, *AJ*, 139, 2440
- Rosolowsky, E. W., Pineda, J. E., Foster, J. B., et al. 2008, *ApJS*, 175, 509
- Sadavoy, S. I., Di Francesco, J., André, P., et al. 2014, *ApJ*, 787, L18
- Siess, L., Dufour, E., & Forestini, M. 2000, *A&A*, 358, 593
- Skrutskie, M. F., Cutri, R. M., Stiening, R., et al. 2006, *AJ*, 131, 1163
- Tu, X., & Wang, Z.-X. 2013, *Research in Astronomy and Astrophysics*, 13, 323
- Willis, S., Marengo, M., Allen, L., et al. 2013, *ApJ*, 778, 96
- Wright, E. L., Eisenhardt, P. R. M., Mainzer, A. K., et al. 2010, *AJ*, 140, 1868